

1           **Drought-Induced Soil Carbon Dynamics in Subtropical Forests: Emergent**  
2   **Divergence from Model Structures**

3  
4           Fengfeng Du<sup>1</sup>, LianJun Feng<sup>1</sup>, Lingyan Zhou<sup>2</sup>, Zhizhuang Gu<sup>3</sup>, Yaqi Zhang<sup>1</sup>,  
5   Zhenggang Du<sup>1\*</sup>, Xuhui Zhou<sup>1</sup>

6  
7  
8  
9  
10  
11       <sup>1</sup>Northeast Asia ecosystem Carbon sink research Center (NACC), Key Laboratory of  
12           Sustainable Forest Ecosystem Management-Ministry of Education, School of  
13           Forestry, Northeast Forestry University, Harbin, 150040, China

14       <sup>2</sup>Shanghai Engineering Research Center of Sustainable Plant Innovation, Shanghai  
15           Botanical Garden, Shanghai, China

16       <sup>3</sup>Zhejiang Tiantong Forest Ecosystem National Observation and Research Station,  
17           School of Ecological and Environmental Sciences, East China Normal University,  
18           Shanghai, 200062, China

19  
20  
21       \*Corresponding author. Email: [zgdu@nefu.edu.cn](mailto:zgdu@nefu.edu.cn)

23 **ABSTRACT**

24 Accurately quantifying drought impacts on terrestrial carbon cycling is essential for  
25 advancing predictions of climate-carbon feedbacks. However, current biogeochemical  
26 models exhibit limited capability in simulating drought-induced transformations of soil  
27 organic carbon (SOC), particularly regarding microbial processes. Here, we conducted  
28 a systematic comparative evaluation of three prevailing SOC modeling structures,  
29 including conventional three-pool partitioning scheme (SM1), mineral and particulate-  
30 associated carbon partitioning scheme (SM2) and Michaelis-Menten regulated carbon-  
31 stabilization scheme (SM3), to elucidate their capacity in simulating soil carbon  
32 dynamics under decadal drought scenarios in a subtropical forest. We found divergent  
33 effects of drought in soil C input (SM1, 66%; SM2, 10%; SM3, -4%) and mean  
34 residence time (MRT; SM1, -31%; SM2, -14%; SM3, 65%), which lead to the predicted  
35 SOC substantial accumulation for both SM1 and SM3 (+39.5% and +56.9%,  
36 respectively) and moderate depletion (-6.1%) for SM2. Drought leads to a decrease in  
37 microbial carbon and an increase in POC, while the responses of other carbon pools  
38 vary across different models. These findings highlight critical model structural  
39 dependencies in simulating drought-affected soil carbon dynamics and emphasize the  
40 necessity for models to integrate microbial-physicochemical interactions for improved  
41 climate-carbon coupling projections.

42 **Keywords:** soil carbon stock, extreme drought, microbial enzyme activity, model  
43 comparison, data assimilation, traceability analysis.

## 44 **1 Introduction**

45 Terrestrial ecosystems are facing increasing frequent stress from extreme drought  
46 which fundamentally alters plant-microbe-mineral interactions, serving as a key driver  
47 of carbon sequestration patterns (IPCC, 2023; Han et al., 2022; Choat et al., 2018; Hao  
48 et al., 2015). Initial drought exposure typically enhances soil organic carbon (SOC)  
49 stability via physicochemical protection mechanisms, such as reduced microbial  
50 decomposition from moisture limitation (Schimel, 2018), increased organo-mineral  
51 association due to soil contraction (Blankinship et al., 2016), and disrupted enzyme  
52 diffusion (Wu et al., 2025). However, plant-derived carbon inputs decline through  
53 productivity suppression driven by hydraulic failure (Choat et al., 2018) and carbon  
54 allocation shifts away from roots (Yin et al., 2021). Prolonged drought (e.g., >2 years)  
55 induces microbial adaptation strategies which may accelerate SOC loss (Barnard et al.,  
56 2013; Schimel et al., 2018). The shift toward filamentous fungal dominance enhances  
57 oxidative enzyme production, while necromass accumulation primes destabilization of  
58 mineral-associated carbon (Liang et al., 2020; Wang et al., 2024). However, predicting  
59 how terrestrial carbon storage responds to drought over decadal timescales remains a  
60 challenge, requiring the integration of long-term manipulative experiments with models  
61 capable of capturing drought-induced changes in plant-microbe-mineral interactions.

62 In most terrestrial ecosystem models, SOC is typically represented as discrete  
63 compartments defined by their turnover times (Krinner et al., 2005; Lawrence et al.,  
64 2019). Early modeling approaches, such as the single-pool model proposed by Jenny et  
65 al. (1941), treated SOC as a homogeneous system. Subsequent refinements led to the

66 development of multi-pool frameworks. For example, Campbell et al. (1978)  
67 categorized SOC into labile and stable organic matter. The TECO model further  
68 advanced this by partitioning SOC into three pools (fast, slow, and passive SOM) with  
69 different turnover rates (Xu et al., 2006; Du et al., 2017; Wan et al., 2025). Later  
70 developments incorporated greater complexity, such as separating recalcitrant fractions  
71 and accounting for physically protected organic matter, which decomposes more slowly  
72 than unprotected forms (Paul et al., 1978; Willard et al., 2024).

73       Theoretical advancements in soil organic matter (SOM) formation and  
74 decomposition improve the representation of SOC in land-surface and terrestrial  
75 ecosystem models (Basile-Doelsch et al., 2020; Si et al., 2023; Cotrufo et al., 2022;  
76 Sokol et al., 2019). Measured SOC fractions, such as particulate organic carbon (POC),  
77 mineral-associated organic carbon (MAOC) and dissolved organic carbon (DOC), have  
78 been proposed to link conceptual SOC pools (Lee et al., 2020). POC is typically  
79 considered as fragments of plant residues with a particle size  $> 53 \mu\text{m}$ , and it is more  
80 susceptible to external environment changes (Cotrufo et al., 2019; Benbi et al., 2014;  
81 Lugato et al., 2022). MAOC generally consists of microbial and plant-derived organo-  
82 mineral complexes rich in nutrients, typically  $< 53 \mu\text{m}$ , while also being associated  
83 with minerals and embedded in soil aggregates (Si et al., 2023; Hansen et al., 2024;  
84 Villarino et al., 2021). Some studies have revealed that models constrained by  
85 measurable SOC pools can provide more accurate estimation of model parameters  
86 thereby more accurate projections of SOC dynamics (Guo et al., 2022; Tao et al., 2024;  
87 Abramoff et al., 2022). Dissolved organic carbon (DOC), derived from living roots or

88 transformed from recalcitrant macromolecular organic matter, is approximately 2 to 3  
89 times more efficient than litter in forming SOM (Sokol et al., 2019; Cotrufo et al., 2013).  
90 Moreover, the adsorption and desorption processes of DOC represent a key link in SOC  
91 decomposition (Camino-Serrano et al., 2018; Wu et al., 2014). Consequently,  
92 incorporating DOC and its interaction with SOC into models represents a crucial  
93 advance.

94 Soil organic matter decomposition is a stepwise process in which microbes secrete  
95 extracellular enzymes to catalyze the substrate, converting SOM into assimilable  
96 subunits (Caldwell et al., 2005; Szejgis et al., 2024). Extensive manipulative  
97 experiments reveal that short-term drought limits microbial activities and substrate  
98 decomposition rates by inducing osmotic stress and constraining substrate diffusion  
99 (Honeker et al., 2024; Citerne et al., 2021). In contrast, long-term drought alters  
100 microbial community structure and carbon utilization patterns (Hueso et al., 2012;  
101 Preece et al., 2019; Wang et al., 2024). As catalysts of decomposition, microbial enzyme  
102 activities are impacted by drought (Sardans et al., 2010; Stursova et al., 2012; Wu et al.,  
103 2025). For example, drought significantly reduces the activities of  $\beta$ -glucosidase, acid  
104 phosphatase and polyphenol oxidase, although certain oxidases remain unaffected by  
105 soil moisture (Su et al., 2020a; Allison et al., 2023; Ficken & Warren., 2019). In recent  
106 years, microbial models, which focus on the process of microbial decomposition, have  
107 become increasingly incorporated in process-based ecological models (Moorhead et al.,  
108 2006; Lawrence et al., 2009; Allison et al., 2010; Huang et al., 2018).

109        Despite these advancements, a critical knowledge gap remains: how structural  
110        uncertainty, fundamentally different assumptions about carbon stabilization, leads to  
111        divergent projections of SOC response to decadal drought which refers to continuously  
112        reduced approximately 70% of natural rainfall sustained for over a decade (Su et al.,  
113        2020a). Traditional three-pool models feature conceptually unmeasurable carbon pools,  
114        and predictions of SOC rely solely on parameterization of total SOC (Guo et al., 2022),  
115        which obscures the responses of different carbon fractions (POC, MAOC, DOC) to  
116        drought and may lead to substantial errors in long-term projections. Furthermore,  
117        current models rarely explicitly represent the direct regulation of SOC by specific  
118        microbial enzymes and the effects of prolonged drought (Luo et al., 2020; Knorr et al.,  
119        2005; Eastman et al., 2024). Emerging frameworks that incorporate measurable  
120        fractions or explicit microbial enzyme kinetics (Michaelis-Menten dynamics) offer the  
121        potential to mechanistically represent the processes. However, these approaches differ  
122        fundamentally in their representation of carbon stabilization and decomposition, and no  
123        systematic evaluation has compared their performance against long-term drought  
124        experimental data. Such a comparison is essential, as the choice of model structure may  
125        not only influence predictive accuracy but also shape our mechanistic understanding of  
126        whether drought induces SOC loss or stabilization over decadal timescales.

127        In this study, we evaluate three SOC modeling schemes with increasing complexity,  
128        including conventional three-pool partitioning scheme (SM1), mineral and particulate-  
129        associated carbon partitioning scheme (SM2) and Michaelis-Menten regulated carbon-  
130        stabilization scheme (SM3). Using observational data from long-term drought

131 experiments, we assess their validity and predictive performance. Our study addresses  
132 two key questions: (1) how does decadal drought affect SOC storage in subtropical  
133 forests? (2) do different model structures yield consistent drought impacts on SOC  
134 projections?

135

## 136 **2 Materials and methods**

### 137 **2.1 Site description and data source**

138 The Zhejiang Tiantong Forest Ecosystem National Field Scientific Observation and  
139 Research Station (28°48'N, 121°47'E, 163 m a.s.l) is located in Ningbo, Zhejiang  
140 Province. The site has a typical mid-subtropical monsoon climate with relatively  
141 distinct seasons. Summers are generally mild and rainy, while winters are dry with little  
142 precipitation. The annual average temperature in the study area is approximately  
143 16.2 °C. The annual average precipitation and evaporation are 1384 mm and 1320 mm,  
144 respectively, and the relative air humidity can reach 85%. The predominant soil type in  
145 the site is red-yellow soil and soil parent materials are mainly weathered products of  
146 some granite and sedimentary rocks. The soil texture consists of sand (6.8%), silt  
147 (55.5%), and clay (37.7%), with a pH ranging from about 4.4 to 5.1 (Gao et al., 2014).  
148 The vegetation type in the study area is typical subtropical evergreen broad-leaved  
149 forest, with secondary forests being the main vegetation type. The forest stocking  
150 density is approximately 3400 trees·hm<sup>-2</sup>. The drought experiment was established in  
151 July 2013, which is composed of three experimental plots with similar terrain,  
152 vegetation type and stand condition (Su et al., 2020b).

153 The forcing datasets used in this study span from 2014 to 2022, including  
154 photosynthetically active radiation (PAR), leaf area index (LAI), air temperature (Ta),  
155 relative humidity of air (RH), soil temperature (Ts) and moisture content of soil (SWC).  
156 These data were mainly measured by the station meteorological observation device.  
157 The above-ground biomass data of plants were mainly estimated by allometric growth  
158 equation. The C content of litter was determined by potassium dichromate oxidation  
159 method. Soil total organic carbon and its physical and chemical properties were  
160 measured by elemental analyzer. Microbial biomass carbon was determined by  
161 chloroform fumigation. DOC was determined by hot water extraction and element  
162 analyzer (Zhou et al., 2013). Soil enzyme activities were determined by microplate  
163 enzyme assay (Saiya-Cork et al., 2002; Su et al., 2020b) and was expressed by substrate  
164 conversion per gram of dry soil per hour. The soil respiration rate was measured using  
165 the *LI-COR 8100 portable system* (LI-COR. Inc., Lincoln, NE, USA) between 9 a.m.  
166 and 1 p.m. on 1 - 2 sunny days per month, and accumulated the data on daily scale.

## 167 **2.2 Model description**

168 All three soil models are coupled to a common vegetation submodule (Fig. 1). The  
169 vegetation model simulates photosynthesis and the flow of GPP within vegetation  
170 carbon pools. The photosynthesis process is implemented using the FBEM model,  
171 which is driven by leaf area index, photosynthetically active radiation, air temperature,  
172 and air relative humidity, detailed information can be found in Wu et al (2009).  
173 Vegetation is divided into three carbon pools: foliage, fine roots, and wood. A portion  
174 of GPP is returned to the atmosphere as respiration, while the remaining Net Primary

175 Productivity (NPP) is allocated as a carbon source to the three vegetation carbon pools.  
176 Carbon transferred from these three vegetation pools is directed to two litter pools:  
177 metabolic litter and structural litter. The decomposed carbon from the litter pools serves  
178 as the source for soil carbon pools, which is then input into three soil modules. In this  
179 way, we ensure that the three soil modules share the same meteorological forcing data  
180 and SOC input, thereby facilitating a better analysis of differences arising from model  
181 structure, detailed descriptions can be found in Du et al (2025). In SM1, SOC is divided  
182 into three pools, including (1) a microbial pool with fast turnover; (2) a slow  
183 (chemically protected) pool, and (3) a passive (physically protected) pool (Xu et al.,  
184 2006; Du et al., 2015). In SM2, SOC is divided into four pools (Si et al., 2023),  
185 including (1) a dissolved organic carbon pool (DOC), which is converted from organic  
186 matter with high molecular weight and difficult to decompose. Microbes can utilize  
187 DOC and release CO<sub>2</sub> (Allison et al., 2010; Lawrence et al., 2009); (2) a microbial pool;  
188 (3) a particulate organic carbon pool (POC), and (4) a mineral- associated organic  
189 carbon (MAOC). SM3 is an extension of SM2 that incorporates three enzyme  
190 components:  $\beta$ -1, 4-glucosidase (BG), polyphenol oxidase (PPO), and  
191 cellobiohydrolase (CBH). These three enzymes provide a parsimonious yet functionally  
192 representative set for capturing drought effects on SOC decomposition (Chen et al.,  
193 2018). BG and CBH are primarily involved in the depolymerization of cellulose and  
194 labile carbon compounds, while PPO is associated with the oxidation of more  
195 recalcitrant substrates such as lignin-like compounds (Su et al., 2020b). Together, these  
196 enzymes capture the rate-limiting steps of both labile and resistant carbon

197 decomposition. Given that enzymes have a low carbon content and their inclusion a  
 198 pool could lead to model overparameterization, we therefore assign them a catalysis  
 199 role instead of considering them as carbon pools. In these three model schemes, SM1  
 200 and SM2 implicitly represent microbial activities, where the decomposition of SOM  
 201 governed by linear, first- order dynamics. Soil C turnover times are defined by biome  
 202 and pool-specific decay constants, which are modified by environmental scalars such  
 203 as soil temperature and soil moisture availability (Du et al., 2017; Du et al., 2025). In  
 204 contrast, the SM3 adopted reverse Michaelis-Menten kinetics to explicitly represent the  
 205 catalytic progress of microbial extracellular enzymes. The turnovers of DOC, POC and  
 206 MAOC are depended on the size of both the donor (substrate) and the receiver  
 207 (microbial biomass) pools. SM1 was expressed by the following equations:

$$208 \quad \frac{dC_M}{dt} = I + C_S c_7 a_{67} + C_P c_8 a_{68} - C_M c_6 \quad (1)$$

$$209 \quad \frac{dC_S}{dt} = I + C_M c_6 a_{76} - C_S c_7 \quad (2)$$

$$210 \quad \frac{dC_P}{dt} = C_M c_6 a_{86} + C_S c_7 a_{87} - C_P c_8 \quad (3)$$

211 Where  $C_M$ ,  $C_S$ ,  $C_P$  represent the C content of microbe, slow SOM and passive SOM.  $I$   
 212 represents the C input from litters,  $c_6$ ,  $c_7$ ,  $c_8$  represent the exit rate of C from microbes,  
 213 slow SOM and passive SOM, and  $a_{67}$ ,  $a_{68}$ ,  $a_{76}$ ,  $a_{78}$  represent the allocation of slow SOM  
 214 to microbes, passive SOM to microbes, microbes to slow SOM and passive SOM to  
 215 slow SOM, respectively.

216 The soil C pools of SM2 were expressed as follows:

$$217 \quad \frac{dC_{DOC}}{dt} = I + C_{POC} c_7 a_{67} + C_{MAOC} c_9 a_{69} - C_{DOC} c_6 \quad (4)$$

$$218 \quad \frac{dC_{POC}}{dt} = I + C_M c_8 a_{78} - C_{POC} c_7 \quad (5)$$

$$219 \quad \frac{dC_M}{dt} = C_{DOC} c_6 a_{86} - C_M c_8 \quad (6)$$

$$220 \quad \frac{dC_{MAOC}}{dt} = C_{POC} c_7 a_{97} + C_M c_8 a_{98} - C_{MAOC} c_9 \quad (7)$$

221 Where  $C_{DOC}$ ,  $C_{POC}$ ,  $C_{MAOC}$  represent the C content of DOC, POC, MAOC. Parameters  
 222  $c_6$ ,  $c_7$ ,  $c_8$ ,  $c_9$  denote the exit rate of DOC, POC, microbes and MAOC, and  $a_{67}$ ,  $a_{69}$ ,  $a_{78}$ ,  
 223  $a_{86}$ ,  $a_{97}$ ,  $a_{98}$  represent the allocation of POC to DOC, MAOC to DOC, microbes to POC,  
 224 DOC to microbes, POC to MAOC and microbes to MAOC, respectively. SM3 was  
 225 expressed by the following equations:

$$226 \quad \frac{dC_{DOC}}{dt} = I + a_{67}(V_{CBH.P} + V_{PPO.P} + V_{BG.P})C_{POC} +$$

$$a_{69}(V_{CBH.M} + V_{PPO.M} + V_{BG.M})C_{MAOC} - \frac{V_{max.assim}C_M C_{DOC}}{KM_{assim} + C_{DOC}} \quad (8)$$

$$227 \quad \frac{dC_{POC}}{dt} = I + C_M c_8 a_{78} - (V_{CBH.P} + V_{PPO.P} + V_{BG.P})C_{POC} \quad (9)$$

$$228 \quad \frac{dC_M}{dt} = C_{DOC} c_6 a_{86} - C_M c_8 \quad (10)$$

$$229 \quad \frac{dC_{MAOC}}{dt} = a_{97}(V_{CBH.P} + V_{PPO.P} + V_{BG.P})C_{POC} + a_{98}c_8C_M$$

$$-(V_{CBH.M} + V_{PPO.M} + V_{BG.M})C_{MAOC} \quad (11)$$

230 Where  $V_{max.assim}$  and  $KM_{assim}$  denote microbe maximum assimilation rate and half-  
 231 saturation for assimilation.  $V_{CBH.P}$ ,  $V_{PPO.P}$ ,  $V_{BG.P}$  represent catalytic rate of CBH, PPO,  
 232 BG to POC.  $V_{CBH.M}$ ,  $V_{PPO.M}$ ,  $V_{BG.M}$  represent catalytic rate of CBH, PPO, BG to MAOC.

$$233 \quad V_{enzyme.P} = \frac{V_{max.enzyme}f_{enzyme}C_M}{KM_{enzyme} + C_{POC}} \quad (12)$$

$$234 \quad V_{enzyme.M} = \frac{V_{max.enzyme}f_{enzyme}C_M}{KM_{enzyme} + C_{MAOC}} \quad (13)$$

235 Where  $V_{max.enzy}$  represent the maximum reaction rate.  $KM_{enzy}$  represent half-saturation  
236 for reaction,  $f_{enzy}$  represent the C ratio of CBH, PPO, BG to microbes, respectively. The  
237 enzyme activities were calculated as following:

$$238 \quad V_{enzy} = \frac{V_{max.enzy} f_{enzy} C_M C_{sub}}{KM_{enzy} + C_{sub}} \quad (14)$$

239 Where  $C_{sub}$  denotes the C content of the enzyme-catalyzed substrate contained within  
240 a soil block with an area of 1 m<sup>2</sup> and a depth of 10 cm, and it maintains a consistent  
241 ratio of enzyme to substrate as required for experimental measurements.

242 To quantify model uncertainty, we employed the MCMC data assimilation method  
243 (Xu et al., 2006) to invert model parameters (Table A1). Subsequently, 1,000 sets of  
244 parameters were randomly sampled from the posterior distribution of each parameter  
245 to generate predictions (Fig. 3). The standard deviation of the 1,000 simulation results  
246 for total organic carbon (TOC) in the year 2100 from each model was used to represent  
247 the magnitude of uncertainty arising from model parameters. The traceability analysis  
248 framework (Supplement) was used to evaluate changes in the simulated ecosystem C  
249 storage capacity. The effect of drought on C storage is calculated as follows:

$$250 \quad Drought\ Effect = \frac{(C_{drought} - C_{ctr})}{C_{ctr}} \times 100\% \quad (15)$$

251 Where  $C_{drought}$  represents the C content of drought,  $C_{ctr}$  represents the C content of  
252 control condition.

253

## 254 **3 Results**

### 255 **3.1 Model validation**

256 In this study, we used the Markov Chain Monte Carlo (MCMC) algorithm to constrain  
257 model parameters (Figs. 2 and A3). All schemes incorporate 8 vegetation-related  
258 parameters (Fig. A3). SM1 included 8 soil carbon-related parameters (Fig. 2), with 5  
259 well-constrained under control conditions ( $c_7, a_{86}, a_{67}, a_{87}, a_{68}$ ) and 5 under drought  
260 conditions ( $c_7, c_8, a_{76}, a_{86}, a_{68}$ ). SM2 consisted 14 soil carbon-related parameters, with  
261 7 well-constrained in the control scenario ( $c_9, c_{10}, a_{74}, a_{65}, a_{67}, a_{97}, a_{78}$ ) and 9 in the  
262 drought scenario ( $c_9, c_{10}, a_{64}, a_{74}, a_{86}, a_{67}, a_{97}, a_{98}, a_{69}$ ). SM3 had 11 well-constrained  
263 parameters under control conditions ( $V_{max.assim}, V_{max.CBH}, KM_{CBH}, f_{CBH}, f_{BG}, f_{PPO}, a_{64}, a_{74},$   
264  $a_{75}, a_{97}, a_{78}$ ) and 12 under drought conditions ( $c_6, V_{max.assim}, V_{max.CBH}, KM_{CBH}, KM_{BG},$   
265  $V_{max.PPO}, KM_{PPO}, f_{BG}, f_{PPO}, a_{65}, a_{86}, a_{97}$ ) in all 22 soil carbon-related parameters.

266 All three schemes calibrated by observations from the drought experimental which  
267 had overall good agreement (Figs. A1 and A2). The simulation of vegetation C (leaf,  
268 fine root, wood) and soil respiration exhibited high accuracy. The simulated MBC by  
269 SM1 was inferior to those simulated by SM2 and SM3, suggesting that incorporating  
270 measurable C pools can improve the accuracy of MBC simulation. By comparing the  
271 accuracy of POC and MAOC, we found that SM3 generally outperformed SM2,  
272 indicating that the incorporation of enzyme activities can enhance the simulation of the  
273 SOC fractions, particularly with respect to MAOC.

### 274 **3.2 Carbon simulation and prediction by three model schemes**

275 Carbon storage from 2023 to 2100 was predicted using three different model schemes.  
276 All models consistently indicated an increasing trend in vegetation C (VegC) and a  
277 decreasing trend in SOC under both control and drought conditions (Figs. 3 and A4).

278 Specifically, under control conditions, SM1 simulated change rates of 260% for VegC,  
279 -56.9% for SOC and 188% for total organic carbon (TOC). Under drought conditions,  
280 the corresponding rates were 223%, -50.4% and 159%. SM2 projected growth rates of  
281 263% for VegC, -60.8% for SOC and 179% for TOC under control conditions, and  
282 217%, -55% and 151% under drought. For SM3, the simulated growth rates were 230%  
283 for VegC, -88% for SOC and 146% for TOC in the control scenario, while under  
284 drought the values were 169%, -55% and 106%, respectively.

285 The coefficient of variation (CV) of predicted TOC in 2100 across 1,000 parameter  
286 sets was 0.12 for SM1, 0.15 for SM2, and 0.22 for SM3. Importantly, the difference  
287 between the highest and lowest median TOC predictions among the three models (SM1,  
288 5.2, SM2, 4.1, SM3, 3.8 kg C m<sup>-2</sup>) is approximately 2.5 times larger than the average  
289 within-model parametric uncertainty (mean SD, 0.6 kg C m<sup>-2</sup>), demonstrating that  
290 model structural uncertainty dominates (Fig. 3j).

### 291 **3.3 Drought effects on carbon storage**

292 All three modeling schemes consistently indicated that drought reduced C content in  
293 MBC (SM1, -36.9%; SM2, -56.9%; SM3, -27.3%), VegC (SM1, -16.8%; SM2, -19.9%;  
294 SM3, -25.4%) and TOC (SM1, -15%; SM2, -19.4%; SM3, -24.4%). However, the  
295 simulated responses of SOC to drought varied among the schemes (Fig. 4). SM1  
296 predicted an increase in SOC under drought conditions (+39.5%) compared to the  
297 control, driving by increases in both the slow (+13%) and passive (+57%) C pools.  
298 Similarly, SM3 projected a rise in SOC (+56.9%), accompanied by increases in POC  
299 (+82.3%), MAOC (+88.1%), and DOC (+6.7%). In contrast, SM2 simulated a decrease

300 in SOC (-6.1%), with reductions in DOC (-35.3%) and MAOC (-3.7%), through POC  
301 increased (+43.4%).

302 By comparing the proportion of drought effects on each carbon pool simulated by  
303 each model to the total drought effects across the three models, it is apparent that  
304 different modeling schemes exhibit distinct sensitivities to drought (Fig. 4). Specifically,  
305 SM2 demonstrated greater sensitivity to drought effects on microbial biomass (-54%)  
306 and DOC (-84%) compared to SM3 (-18% and +16%, respectively). Conversely, SM3  
307 showed higher sensitivity to drought-induced changes on POC (+82%) and MAOC  
308 (+74%) relative to SM2 (-26% and +18%, respectively).

#### 309 **3.4 Traceability analysis of drought effects**

310 The traceability analysis revealed that both SM1 and SM3 simulated higher SOC under  
311 drought condition (SM1, 2.5 kg C m<sup>-2</sup>; SM3, 1.2 kg C m<sup>-2</sup>) compared to the control  
312 (SM1, 2.1 kg C m<sup>-2</sup>; SM3, 0.8 kg C m<sup>-2</sup>) at the end of forecast period (Fig. 5). In contrast,  
313 SM2 simulated lower SOC under drought (2.3 kg C m<sup>-2</sup>) compared to the control (2.5  
314 kg C m<sup>-2</sup>). The increase of SOC in SM1 during drought was driven by higher soil carbon  
315 input (drought, 1.0 kg C m<sup>-2</sup> year<sup>-1</sup>; control, 0.6 kg C m<sup>-2</sup> year<sup>-1</sup>) (Figs. 4), while in SM3,  
316 it resulted from an extended soil carbon residence time (drought, 4.3 years; control, 2.6  
317 years). However, SM2 simulated a reduction in soil carbon residence time under  
318 drought, leading to decreased SOC.

319 We further analyzed the C residence times of individual pools simulated by the three  
320 modeling schemes under both control and drought conditions (Fig. 4c). In SM1, drought  
321 increased the C residence time of passive SOM. For SM2, drought reduced the C

322 residence time of microbes and increased that of MAOC. In SM3, drought resulted in  
323 a longer C residence time for MAOC.

## 324 **4 Discussion**

### 325 **4.1 Response of ecosystem carbon dynamics to long-term drought**

326 In this study, all three modeling schemes consistently indicate that drought leads to  
327 decrease in vegetation carbon, microbes carbon (Microbe C) and total organic carbon  
328 (TOC), while POC increases under drought conditions (Figs. 3, 4 and A4). These  
329 findings are consistent with multiple fields manipulated experiments (Zhou et al., 2020;  
330 Pennisi, 2022; Schwalm et al., 2017). During drought, plants undergo physiologically  
331 adjustments and shifts in community structure in accordance with species-specific  
332 water use strategies to prevent excessive water loss (Rowland et al., 2023). These  
333 responses in turn affect C uptake via photosynthesis and C release via respiration at the  
334 ecosystem level, potentially decoupling these two processes (Meir et al., 2008).

335 Drought consistently reduced microbial biomass carbon (MBC) across all three  
336 models, and sensitivity analysis indicated this reduction was primarily driven by  
337 increased microbial decay rates (Figs. 2 and A5). With prolonged drought duration,  
338 microbial C content exhibited a pattern of initial decline followed by a gradual recovery  
339 (Fig. 3b). Drought-induced water stress directly impairs microorganisms, leading to  
340 decreased metabolic activity (Quiroga et al., 2024). However, microorganisms can  
341 adapt to drought through physiological changes, community turnover, and evolutionary  
342 mechanisms (Martiny et al., 2015; Allison, 2023). At the community scale, drought-  
343 sensitive microbes may be replaced by more resilient taxa that immigrate into the area

344 (Allison et al., 2008; Ricks & Yannarell., 2023). Several studies have showed that fungi  
345 exhibit greater drought adaptability compared to bacteria (Preece et al., 2019; Bastida  
346 et al., 2018; Williams & de Vries et al., 2018). Gram-positive bacteria are also better  
347 adapted to low-moisture soils compared to Gram-negative bacteria, due to their thicker  
348 and harder cell walls, which render them less affected by drought (Castro et al., 2010).  
349 Through in situ manipulation experiments at the same site, Bu et al (2018) and Su et al  
350 (2020b) have observed that drought slightly reduced MBC and microbial biomass  
351 nitrogen (MBN), and significantly altered the microbial community structure. Drought  
352 significantly increased the relative abundance of Acidobacteria, which was primarily  
353 associated with the decrease in soil pH, while the relative abundance of Proteobacteria  
354 decreased significantly. Besides, the red-yellow soil at the Tiantong site is rich in Fe/Al  
355 oxyhydroxides (e.g., hematite, goethite) and kaolinite, which provide a high specific  
356 surface area and strong adsorption capacity for microbial necromass and DOC (Wang  
357 et al., 2025). Given that microbes directly consume DOC, the incorporation of  
358 measured DOC pools in SM2 and SM3 enhances the model's ability to simulate  
359 microbial sensitivity to drought (Fig. 4b).

360 Simulation results from all three modeling schemes consistently showed that drought  
361 initially decreased soil respiration, followed by a subsequently recovery (Fig. 3a). This  
362 trend mirrors variations in microbial carbon content, indicating that drought regulates  
363 soil respiration primarily through its control of microbial biomass (Zhao et al., 2025;  
364 Ficken & Warren., 2019). All three schemes consistently simulated an increase in  
365 particulate organic carbon (POC) under drought (Fig. 4b). This cross-model

366 consistency arises from multiple ecological mechanisms that are represented, albeit  
367 differently, across the three model structures (Du et al., 2015; 2017).

368 First, drought causes plants to allocate more carbon belowground to acquire water,  
369 resulting in the increase in root-to-shoot ratio, root dry weight and root morphological  
370 characteristics (Ulrich et al., 2022; Williams et al., 2020; Reinelt et al., 2023). Tracing  
371 analysis shows that soil carbon input simulated by the three models increased under  
372 drought conditions (Fig. 5d). In situ manipulation experiments found that the specific  
373 root length, specific surface area, and fine root biomass of the four dominant local plant  
374 species (e.g., *Castanopsis sclerophylla*, *Schima superba*, *Castanopsis carlesii*,  
375 *Lithocarpus glaber*) all increased significantly under drought stress (Jiang et al., 2023).  
376 This root-derived carbon input is a direct source of POC, as coarse root litter and  
377 particulate root fragments are physically classified as POC. In SM1, this increased input  
378 enters the slow SOM pool, which functionally overlaps with POC in terms of turnover  
379 time and substrate quality (Fig. 5). In SM2 and SM3, these inputs are explicitly routed  
380 to the POC pool via litter transfer coefficients ( $a_{74}$ ,  $a_{75}$ ).

381 Second, drought suppresses microbial decomposition activity (Feng et al., 2025).  
382 Reduced soil moisture limits extracellular enzyme diffusion, lowers microbial  
383 metabolic efficiency, and decreases the activities of POC-degrading enzymes such as  
384 cellobiohydrolase and  $\beta$ -glucosidase (Su et al., 2020b; Wu et al., 2025). This  
385 suppression is represented in SM1 and SM2 indirectly through soil moisture scalar  
386 functions that reduce decomposition rates of all pools, whereas SM3 explicitly captures

387 the reduction via enzyme kinetic parameters ( $V_{max}$ ,  $KM$ ) and enzyme-to-microbial  
388 carbon ratios ( $f_{CBH}$ ,  $f_{BG}$ ,  $f_{PPO}$ ).

389 Third, drought-induced changes in soil physicochemical properties suppress the  
390 decomposition of SOC. Drought-induced soil aggregate dynamics may physically  
391 protect POC from decomposition. Although not explicitly modeled in any of the three  
392 schemes, the net effect of reduced POC loss relative to input is emergent in all three  
393 model structures. The correlation between soil physicochemical properties and soil  
394 carbon mineralization rates indicates that soil moisture content, total carbon (TC), total  
395 phosphorus (TP), inorganic nitrogen (IN), available phosphorus (available-P), TC/TP,  
396 TN/TP, and IN/available-P are key factors. Soil carbon mineralization rates are  
397 positively correlated with soil moisture content, TC/TP, TN/TP, and IN/available-P.  
398 Drought led to a decrease in these physicochemical properties. In contrast, soil carbon  
399 mineralization rates are negatively correlated with available-P, which increases under  
400 drought conditions (Su et al., 2020a).

#### 401 **4.2 Divergent simulations of drought effect on SOC among three modeling** 402 **schemes**

403 A key divergence among the three modeling schemes lies in their simulation of drought  
404 effects on SOC components, which is the key source of discrepancy in the projected  
405 carbon storage response (Figs. 4). SM1 divides SOC into three pools, including MBC,  
406 slow SOM, and passive SOM. However, since only total SOC data are available to  
407 constrain the model, the predictions of this scheme are highly sensitive to the quality  
408 and the duration of SOC observations. Given the non-linear response of ecosystems to

409 drought duration (Müller et al., 2022; Anderegg et al., 2020; Schwalm et al., 2017),  
410 models constrained by short-term observation data may introduce substantial deviation  
411 in long-term projections. In contrast, SM2 partitions the SOC into four observable  
412 carbon pools (i.e., Microbes, POC, MAOC and DOC), each independently constrained  
413 by corresponding measurements. The trajectory of SOC is thus jointly determined by  
414 these four fractions, leading to pronounced differences between the predictions of SM1  
415 and SM2. Given that both models use the same SOC data, this highlights the profound  
416 influence of carbon partitioning strategies on model predictions. Furthermore, drought  
417 causes the carbon input rates and carbon loss rates of individual carbon pools in SM2  
418 deviate from the overall SOC change rate. These pool-specific discrepancies cause the  
419 SOC predictions to diverge increasingly over time between models with different  
420 structures.

421 The differences between SM2 and SM3 are mainly reflected in the dynamics of DOC  
422 and MAOC. SM2 employs first-order linear kinetics to describe the decomposition of  
423 DOC and MAOC, where the decomposition rate is proportional to their C content. In  
424 contrast, SM3 uses reverse Michaelis-Menten kinetics, meaning that SOC  
425 decomposition depends not only on substrate carbon content but also on microbial  
426 biomass and enzyme activities (Chandel et al., 2023). Under drought, SM2 simulates a  
427 decrease in DOC, while SM3 predicts an increase (Fig. 4). Some studies report that  
428 drought reduces DOC concentrations (Tiwari et al., 2022; Wu et al., 2023), whereas  
429 others suggest it may increase DOC due to factors such as air temperature, soil  
430 temperature, humidity, precipitation, pH, and sulfate concentrations (Evans et al., 2005;

431 Sowerby et al., 2010). Sensitivity analysis reveals that DOC in SM2 is influenced  
432 mainly by the transfer ratios of POC to DOC and metabolic litter to DOC (Fig. A5).  
433 However, in SM3, DOC dynamics are primarily controlled by the microbe maximum  
434 assimilation rate and half-saturation for assimilation, indicating that SM3 captures  
435 direct microbial regulation of DOC decomposition. Similarly, while SM2 simulates a  
436 slight decrease in MAOC under drought, SM3 predicts an increase (Fig. 4). This  
437 discrepancy stems the fact that SM3 explicitly incorporates the catalytic effects of three  
438 enzyme activities (BG, PPO and CBH) on MAOC decomposition. Long-term drought  
439 at this site drives a shift toward fungal-dominated microbial communities (Bu et al.,  
440 2018; Su et al., 2020b). Fungi are major producers of oxidative and hydrolytic enzymes  
441 (PPO, CBH, BG). SM3 explicitly represents these enzymes, thereby capturing  
442 drought-induced declines in catalytic rates and MAOC accumulation—a key  
443 mechanism absent in SM2’s implicit microbial representation. This explains why SM3  
444 outperforms SM2 in simulating POC and MAOC dynamics (Fig. A2) and highlights  
445 the importance of integrating microbial physiology and site-specific mineralogical and  
446 ecological traits into SOC models.

### 447 **4.3 Implications for future research and model development**

448 Our study enhances the understanding how drought affects forest C dynamic across  
449 different model schemes. Nevertheless, we acknowledge that several uncertainties  
450 involved in our analysis. First, we only considered three enzymes that directly catalyze  
451 soil carbon decomposition. Other enzymes (e.g., Acid phosphatase, N-acetyl-  
452 glycosaminidase, Peroxidase) may also contribute indirectly to this process (Su et al.,  
453 2020b), but they were not included because their primary roles are in nutrient cycling.

454 Including them would substantially increase model complexity and parameter  
455 identifiability issues, especially given the lack of direct constraints from available  
456 enzyme activity data. Second, when calculating enzyme activities, we applied  
457 laboratory-derived proportional relationships between enzyme quantity and substrate  
458 quantity to field conditions, which assumes substrate availability far exceeds enzyme  
459 availability in field soils. Finally, laboratory enzyme activity measurements typically  
460 use specific substrates, whereas field soils contain multiple potential substrates that  
461 could be catalyzed, which introduces additional uncertainty in our simulations.

462 Although our results demonstrate that incorporating measurable carbon pools or  
463 increasing model complexity can improve simulation accuracy for specific carbon  
464 fractions and capture nonlinear drought responses, this does not imply that all land  
465 surface models should adopt the SM2 or SM3. The appropriate model selection depend  
466 on research objectives, data availability, and computational constraints. Specifically,  
467 SM1 remains sufficient for large-scale simulations and long-term carbon budget  
468 assessments. SM2 is preferable when the goal is to investigate the dynamics of carbon  
469 fractions (e.g., POC, MAOC, DOC) and their compositional changes. SM3 becomes  
470 essential for exploring nonlinear ecosystem responses to extreme climate events such  
471 as drought, warming, or other perturbations. Particularly, the advantages of SM2 and  
472 SM3 are contingent upon the availability of observational data for model calibration.  
473 Without sufficient constraints, increased complexity can lead to greater parameter  
474 uncertainty and reduced robustness. Therefore, future model development should

475 pursue a balanced strategy, introducing additional process representations only when  
476 they are supported by data and justified by the specific application.

## 477 **5 Conclusions**

478 Accurately simulating drought impacts on soil carbon dynamics is critical for predicting  
479 terrestrial carbon sequestration. In this study, we integrated data assimilation and  
480 traceability analysis to evaluate three soil carbon decomposition schemes, examining  
481 how different model structures simulate soil carbon responses to drought. Our results  
482 revealed significant disparities in drought effects on soil organic carbon (SOC) among  
483 the three models, with these differences primarily driven by variations in carbon input  
484 and carbon residence times across pools. Explicitly incorporating microbial enzyme  
485 activities notably altered the impacts of drought on mineral-associated organic carbon  
486 and dissolved organic carbon. These findings underscore the critical roles of carbon  
487 pool partitioning schemes, their empirical constrainability, and the consideration of  
488 microbial enzyme catalytic processes in simulating SOC response to drought, thereby  
489 advancing our understanding of the complex mechanism governing drought-induced  
490 soil organic carbon dynamics.

491

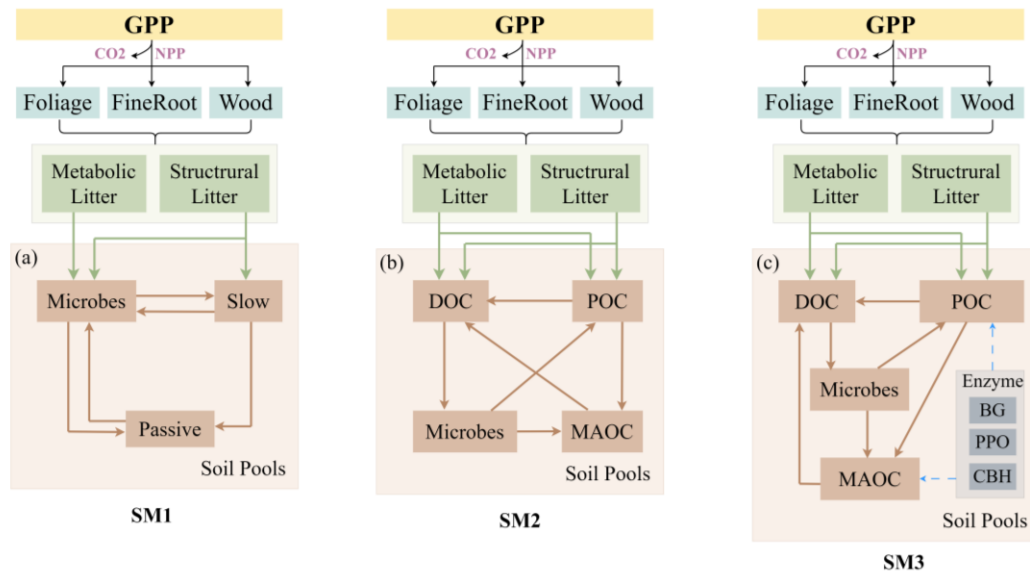
492 **Acknowledgments:** This research was financially supported by the National Natural  
493 Science Foundation of China (Grant No. 32241032, 31930072, 32471683, 32071593)  
494 and the Fundamental Research Funds for the Central Universities (Grant No.  
495 2572022BA08); Heilongjiang Touyan Innovation Team Program (Forest Carbon Sink  
496 Assessment and Carbon Sequestration Management Innovation Team).

497 **CRedit author contribution statement:** F.D and Z.D. collected and analyzed the data  
498 and wrote the manuscript. Z.D. conceived, designed, and oversaw the study. F.D., L.F.,  
499 and Z.G. conducted the statistical analysis. F.D., X.Z., and Z.D. discussed, wrote, and  
500 revised the manuscript with major contributions from L.Z. Y.Z. and G.Z. commented  
501 on the manuscript.

502 **Competing interest declaration:** Authors declare that they have no competing  
503 interests.

504 **Data and materials availability:** Data will be made available on request.

505



506

507 **Figure 1.** Conceptual diagram of the soil biogeochemical models with three schemes.

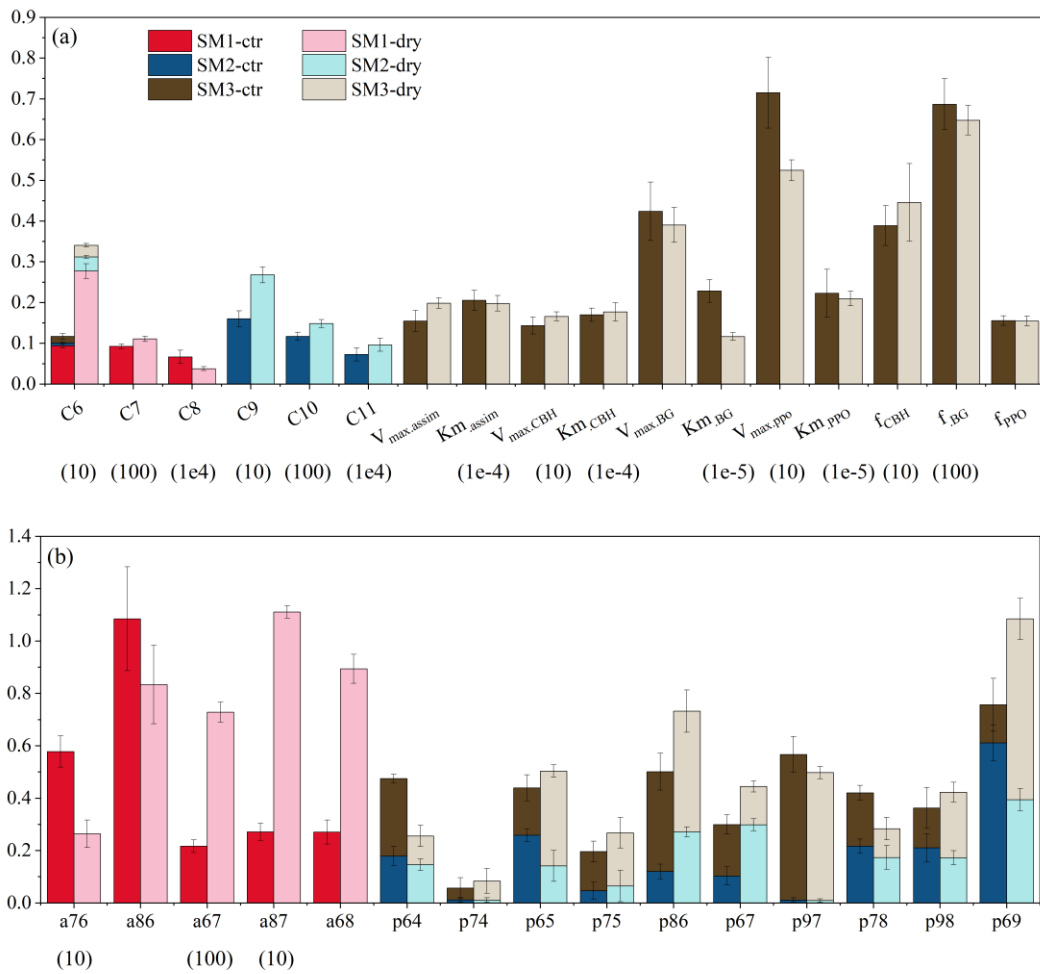
508 **(a)** conventional three-pool partitioning scheme (SM1), **(b)** mineral and particulate-

509 associated carbon partitioning scheme (SM2), and **(c)** Michaelis-Menten regulated

510 carbon-stabilization scheme (SM3). All pools (boxes) and fluxes (arrows) represent C

511 process. BG,  $\beta$ -1, 4-glucosidase, PPO, polyphenol oxidase, CBH, cellobiohydrolase.

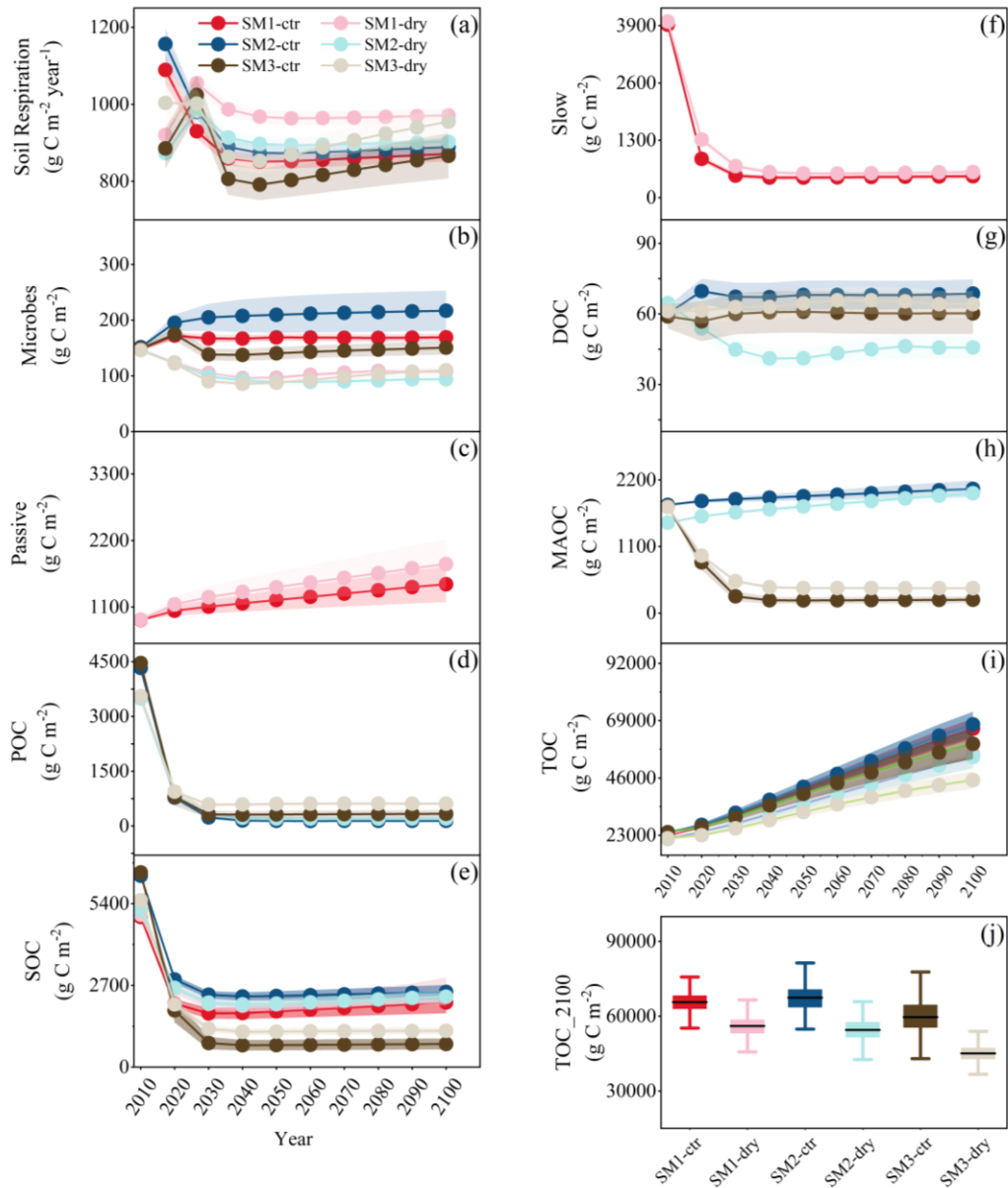
512



514

515 **Figure 2.** Maximum likelihood estimates (MLEs; or means for unconstrained  
 516 parameters) of the target parameters under control and drought treatments across the  
 517 three schemes. Error bars indicate standard deviations (SDs). Refer to Table A1 for  
 518 parameter abbreviations and units.

519



520

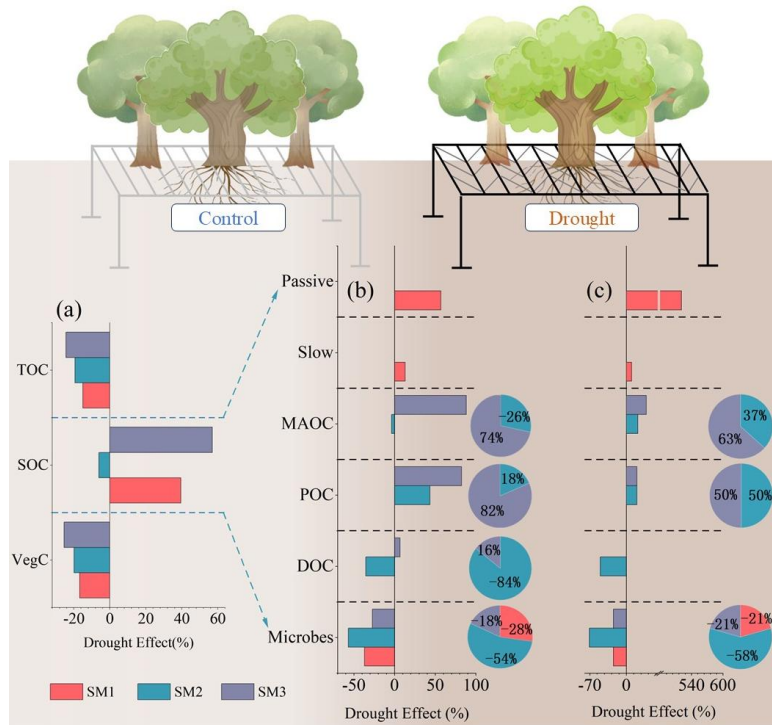
521 **Figure 3.** Predicted soil respiration (a), microbial C (b), passive SOM (c), POC (d),

522 SOC (e), slow SOM (f), DOC (g), MAOC (h), total organic C (i) from 2014 – 2100

523 under dry and control conditions for the three schemes, and (j) the mean TOC in 2100

524 predicted by 1000 simulations.

525

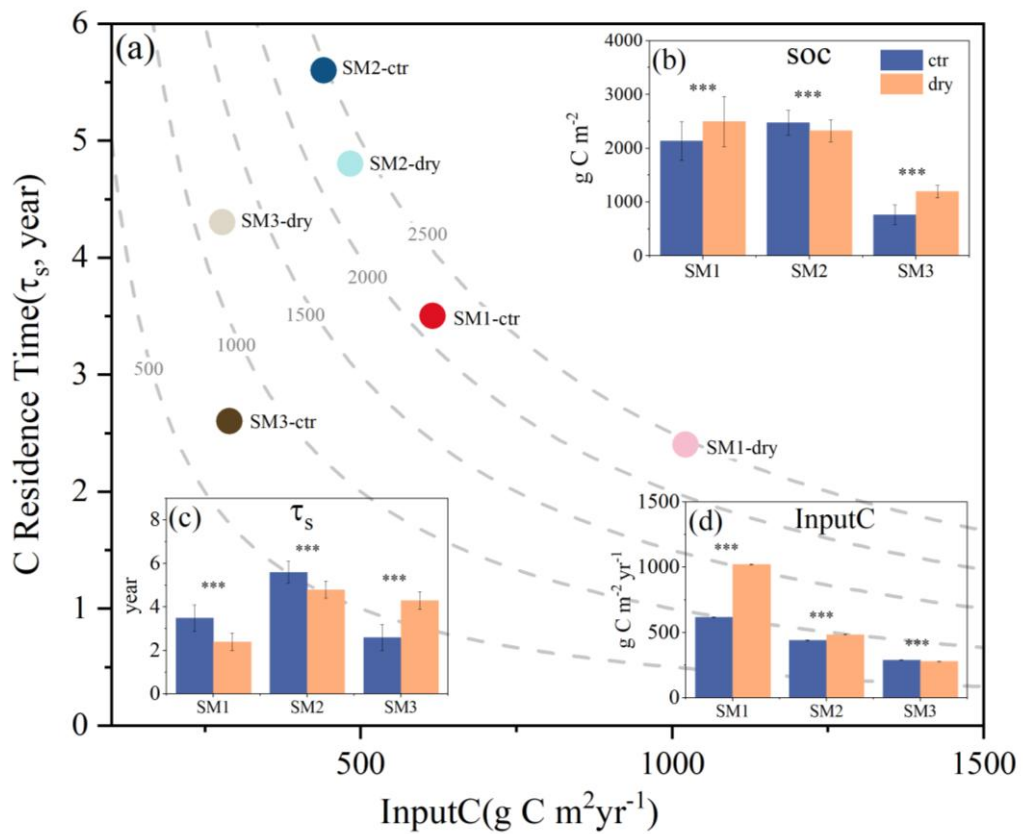


526

527 **Figure 4.** Conceptual diagram illustrating the effects of drought simulated by the three  
 528 schemes on carbon stocks. (a) Drought effects on soil total organic carbon (TOC), soil  
 529 organic carbon (SOC), and vegetation carbon (VegC) in 2100. (b) Drought effects on  
 530 individual carbon pools; pie charts indicate the proportional contribution of each  
 531 scheme to the total drought effect on each pool. (c) Drought effects on carbon residence  
 532 time across pools; pie charts represent the proportional contribution of each scheme to  
 533 the total drought effect on the carbon residence time of each pool.

534

535

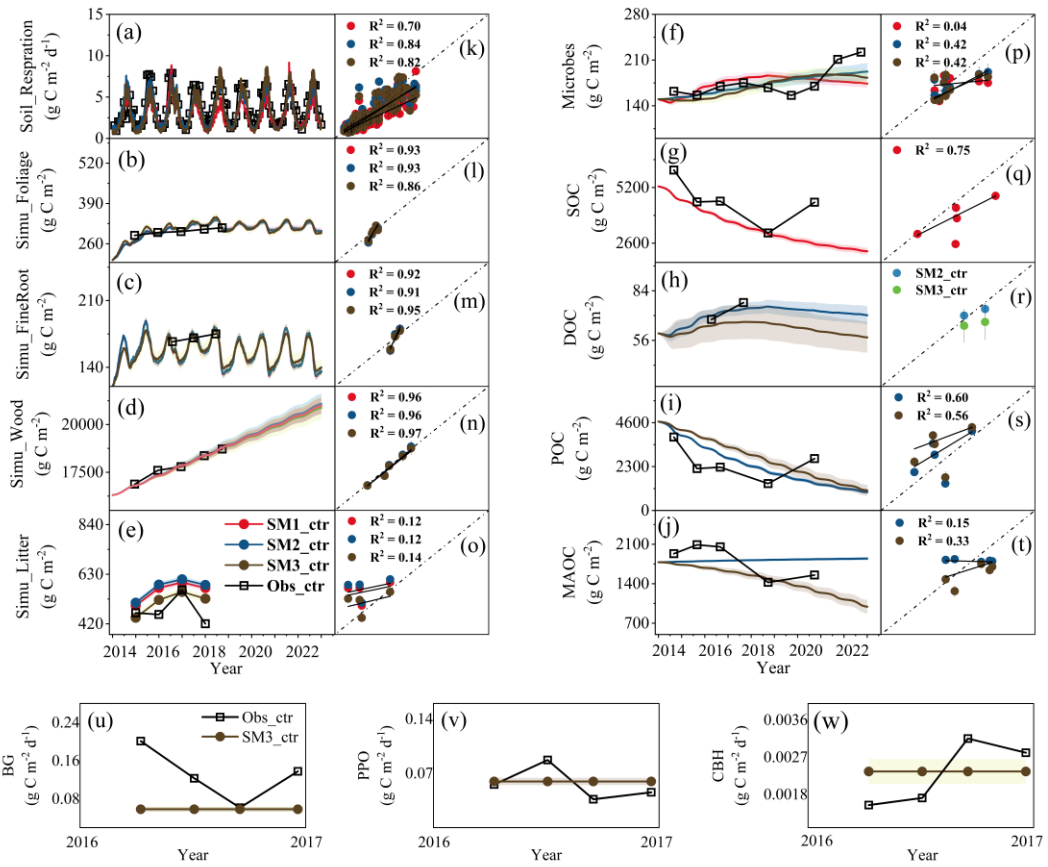


536

537 **Figure 5.** Predicted soil C storage capacity in 2100 by C influx (InputC, x axis) and soil  
 538 carbon residence time ( $\tau_s$ , y axis) between control and drought treatments in three model  
 539 schemes. \*\*\*, represents  $p < 0.01$ .  
 540

541

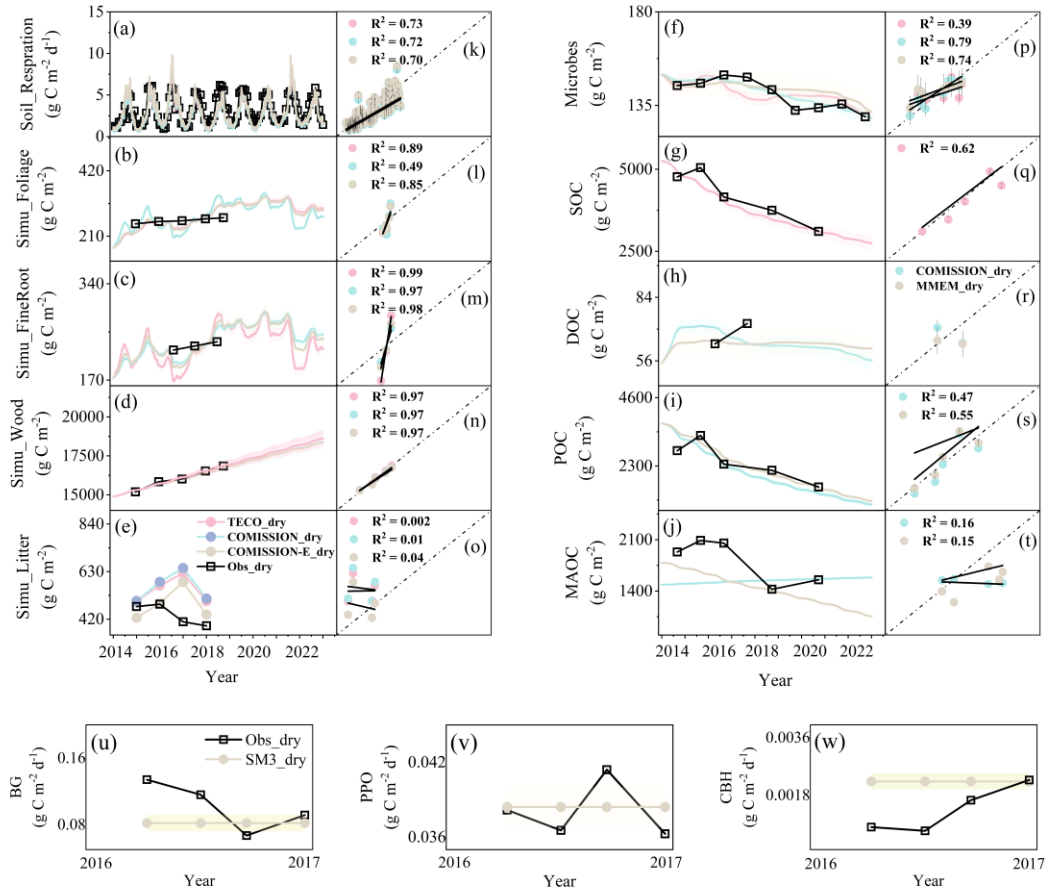
542 Appendix



543

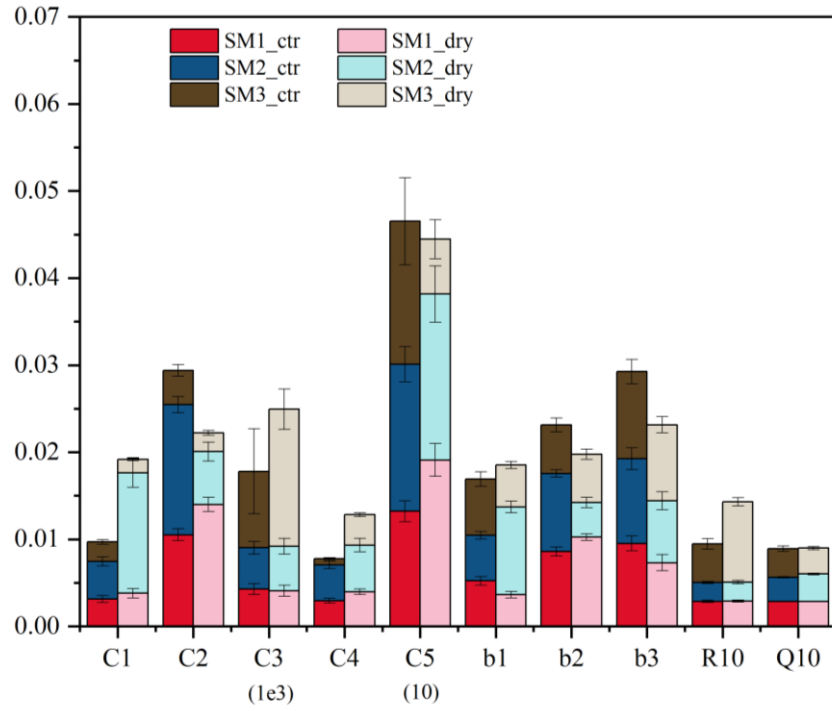
544 **Figure A1.** Comparison of the measured values (black squares) and simulated values  
545 (lines) in the control conditions of three schemes from 2014 to 2022,  $p < 0.05$ .

546



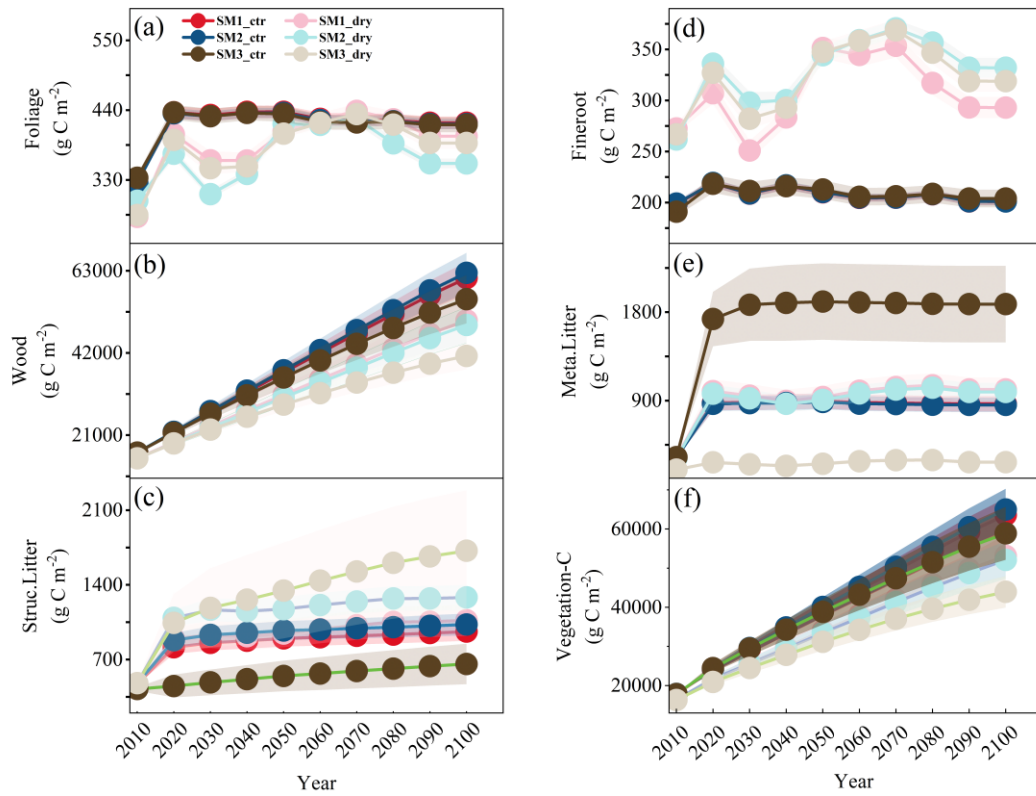
547

548 **Figure A2.** Comparison of the measured values (black squares) and simulated values  
 549 (lines) in the drought conditions of three schemes from 2014 to 2022,  $p < 0.05$ .



550  
 551  
 552  
 553  
 554

**Figure A3.** Maximum likelihood value (MLEs) (or means for unconstrained parameters) of the target parameters of vegetations in various models and treatments. Error bars represent standard deviations (SDs). See Table S1 for parameter abbreviations and units.



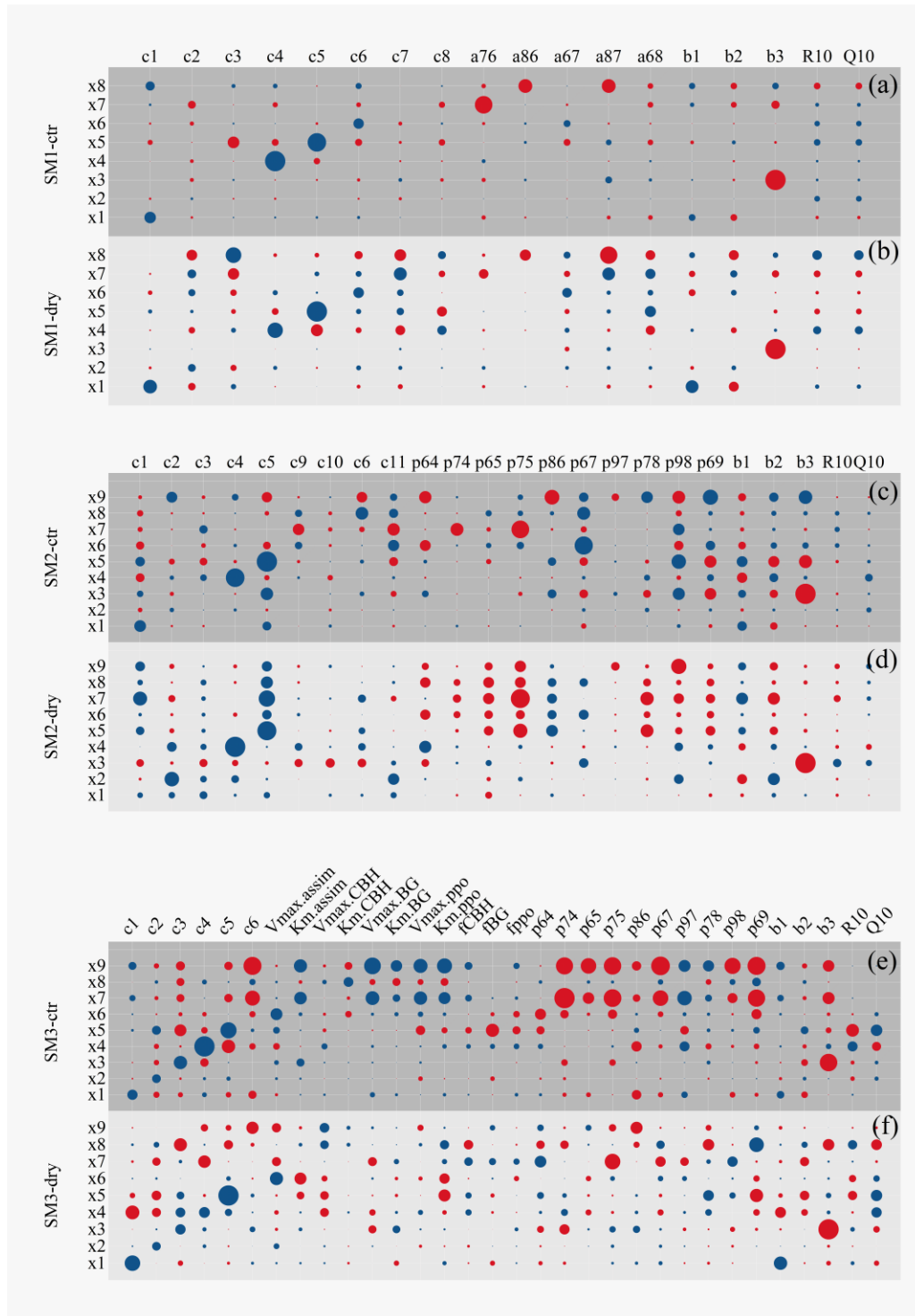
555

556 **Figure A4.** Predicted foliage (a), wood (b), structural litter (c), fineroot (d), Metabolic  
 557 litter (e), Vegetation C (f) from 2014 – 2100 under dry and control conditions for three  
 558 schemes.

559

560

561



562

563 **Figure A5.** The correlation between carbon pools and model parameters under control  
 564 and drought conditions of three schemes. Red represents positive correlation and blue  
 565 represents negative correlation. The  $x1$ ,  $x2$ ,  $x3$ ,  $x4$ ,  $x5$  represent the carbon content of  
 566 foliage, fineroot, wood, metabolic litter, structural litter.  $x6$ ,  $x7$ ,  $x8$  represent microbes  
 567 slow SOM and passive SOM for SM1.  $x6$ ,  $x7$ ,  $x8$ ,  $x9$  represent DOC, POC, microbes  
 568 and MAOC for SM2 and SM3.

569

571 **Table A1.** Target parameters of this study and their prior ranges.

Parameters	Intervals	Unit	Description
<i>C1</i>	0.176-9.95	mg C g <sup>-1</sup> d <sup>-1</sup>	exit rate of C from foliage
<i>C2</i>	0.176-17.9	mg C g <sup>-1</sup> d <sup>-1</sup>	exit rate of C from fineroot
<i>C3</i>	0.00176-0.01	mg C g <sup>-1</sup> d <sup>-1</sup>	exit rate of C from wood
<i>C4</i>	0.274-8.22	mg C g <sup>-1</sup> d <sup>-1</sup>	exit rate of C from metabolic litter
<i>C5</i>	0.0548-1.64	mg C g <sup>-1</sup> d <sup>-1</sup>	exit rate of C from structural litter
<i>C6</i>	2.74-13.7	mg C g <sup>-1</sup> d <sup>-1</sup>	exit rate of C from microbes
<i>C7</i>	0.027-1.37	mg C g <sup>-1</sup> d <sup>-1</sup>	exit rate of C from slow SOM
<i>C8</i>	0.00137-0.00913	mg C g <sup>-1</sup> d <sup>-1</sup>	exit rate of C from passive SOM
<i>C9</i>	2.74-68.5	mg C g <sup>-1</sup> d <sup>-1</sup>	exit rate of C from DOC
<i>C10</i>	0.1-1	mg C g <sup>-1</sup> d <sup>-1</sup>	exit rate of C from POC
<i>C11</i>	0.00137-0.013	mg C g <sup>-1</sup> d <sup>-1</sup>	exit rate of C from MAOC
<i>b1</i>	0-0.315	-	allocation of GPP to foliage
<i>b2</i>	0-0.3	-	allocation of GPP to fineroot
<i>b3</i>	0-0.3	-	allocation of GPP to wood
<i>R10</i>	0-1	g C m <sup>-2</sup> d <sup>-1</sup>	basic respiration rate
<i>Q10</i>	2-5	-	temperature sensitivity of respiration
<i>a76</i>	0-0.5	-	allocation of microbes to slow SOM
<i>a86</i>	0-0.5	-	allocation of microbes to passive SOM
<i>a67</i>	0-0.5	-	allocation of slow SOM to microbes
<i>a87</i>	0-0.5	-	allocation of slow SOM to passive SOM
<i>a68</i>	0-1	-	allocation of passive SOM to microbes
<i>p64</i>	0-0.3	-	allocation of metabolic litter to DOC
<i>p74</i>	0-0.7	-	allocation of metabolic litter to POC
<i>p65</i>	0-0.6	-	allocation of structural litter to DOC
<i>p75</i>	0-0.4	-	allocation of structural litter to POC
<i>p86</i>	0-0.7	-	allocation of DOC to microbes

<i>p67</i>	0-0.8	-	allocation of POC to DOC
<i>p97</i>	0-0.2	-	allocation of POC to MAOC
<i>p78</i>	0-0.7	-	allocation of microbes to POC
<i>p98</i>	0-0.3	-	allocation of microbes to MAOC
<i>p69</i>	0-0.8	-	allocation of MAOC to DOC
$V_{max.assim}$	0.001-0.4	mg C mg <sup>-1</sup> MBC d <sup>-1</sup>	microbe maximum assimilation rate
$Km_{.assim}$	300-3000	g C m <sup>-3</sup>	half-saturation for assimilation
$V_{max.CBH}$	0.0001-0.01	mg C mg <sup>-1</sup> CBH d <sup>-1</sup>	maximum reaction rate of CBH
$Km_{.CBH}$	300-3000	g C m <sup>-3</sup>	half-saturation for reaction of CBH
$V_{max.PPO}$	0.0001-0.2	mg C mg <sup>-1</sup> PPO d <sup>-1</sup>	maximum reaction rate of PPO
$Km_{.PPO}$	300-6000	g C m <sup>-3</sup>	half-saturation for reaction of PPO
$V_{max.BG}$	0.0001-0.2	mg C mg <sup>-1</sup> BG d <sup>-1</sup>	maximum reaction rate of BG
$Km_{.BG}$	300-3000	g C m <sup>-3</sup>	half-saturation for reaction of BG
$f_{CBH}$	0-0.01	-	CBH-to-microbial carbon ratio
$f_{PPO}$	0-0.2	-	PPO-to-microbial carbon ratio
$f_{BG}$	0-0.1	-	BG-to-microbial carbon ratio

---

572

573

574 **References**

- 575 Abramoff, R. Z., Guenet, B., Zhang, H. C., Georgiou, K., Xu, X. F., Rossel, R. A. V.,  
576 Yuan, W. P., and Ciais, P.: Improved global-scale predictions of soil carbon stocks  
577 with Millennial Version 2, *Soil Biol Biochem.*, 164,  
578 <https://doi.org/10.1016/j.soilbio.2021.108466>, 2022.
- 579 Anderegg, WRL., Trugman, AT., Badgley, G., Konings, AG., and Shaw, J.: Divergent  
580 forests sensitivity to repeated extreme droughts, *Nat. Clim. Change.*, 10(12), 1091-  
581 U19, <https://doi.org/10.1038/s41558-020-00919-1>, 2020.
- 582 Allison, S. D.: Microbial drought resistance may destabilize soil carbon, *Trends*  
583 *Microbiol.*, 31(8), 780-787, <https://doi.org/10.1016/j.tim.2023.03.002>, 2023.
- 584 Allison, S. D., and Martiny, J. B. H.: Resistance, resilience, and redundancy in  
585 microbial communities, *PNAS.*, 105, 11512-11519,  
586 <https://doi.org/10.1073/pnas.0801925105>, 2008.
- 587 Allison, S. D., Wallenstein, M. D., and Bradford, M. A.: Soil-carbon response to  
588 warming dependent on microbial physiology, *Nat. Geosci.*, 3(5), 336-340,  
589 <https://doi.org/10.1038/NGEO846>, 2010.
- 590 Basile-Doelsch, I., Balesdent, J., and Pellerin, S.: Reviews and syntheses: The  
591 mechanisms underlying carbon storage in soil, *BIOGEOSCIENCES.*, 17(21),  
592 5223- 5242, <https://doi.org/10.5194/bg-17-5223-2020>, 2020.
- 593 Bastida, F., Torres, I. F., Andrés-Abellán, M., Baldrian, P., López-Mondéjar, R.,  
594 Vetrovsky, T., and Jehmlich, N.: Differential sensitivity of total and active soil  
595 microbial communities to drought and forest management, *Glob Chang Biol.*,  
596 24(1), 552-552, <https://doi.org/10.1111/gcb.13953>, 2018.
- 597 Benbi, D. K., Boparai, A. K., and Brar, K.: Decomposition of particulate organic matter  
598 is more sensitive to temperature than the mineral associated organic matter, *Soil*  
599 *Biol Biochem.*, 70, 183-192, <https://doi.org/10.1016/j.soilbio.2013.12.032>, 2014.
- 600 Blankinship, JC., Fonte, SJ., Six, J., and Schimel, JP.: Plant versus microbial controls  
601 on soil aggregate stability in a seasonally dry ecosystem, *GEODERMA.*, 272(39-  
602 50), <https://doi.org/10.1016/j.geoderma.2016.03.008>, 2016
- 603 Barnard, RL., Osborne, CA., and Firestone, MK.: Responses of soil bacterial and fungal  
604 communities to extreme desiccation and rewetting, *ISME J.*, 7(11), 2229-2241,  
605 <https://doi.org/10.1038/ismej.2013.104>, 2013.
- 606 Bu, X. L., Gu, X. Y., Zhou, X. Q., Zhang, M. Y., Zhang, M. Y., Zhang, J., Zhou, X. H.,  
607 Chen, X. Y., and Wang, X. H.: Extreme drought slightly decreased soil labile  
608 organic C and N contents and altered microbial community structure in a  
609 subtropical evergreen forest, *For. Ecol. Manage.*, 429, 18-27,  
610 <https://doi.org/10.1016/j.foreco.2018.06.036>, 2018.
- 611 Caldwell, B. A.: Enzyme activities as a component of soil biodiversity: A review,  
612 *Pedobiologia.*, 49(6), 637-644, <https://doi.org/10.1016/j.pedobi.2005.06.003>,  
613 2005.
- 614 Camino-Serrano, M., Guenet, B., Luysaert, S., Ciais, P., Bastrikov, V., De Vos, B.,  
615 Gielen, B., Gleixner, G., Jornet-Puig, A., Kaiser, K., Kothawala, D., Lauerwald,

616 R., Peñuelas, J., Schrumpf, M., Vicca, S., Vuichard, N., Walmsley, D., and  
617 Janssens, I. A.: ORCHIDEE-SOM: modeling soil organic carbon (SOC) and  
618 dissolved organic carbon (DOC) dynamics along vertical soil profiles in Europe,  
619 *Geosci. Model Dev.*, 11(3), 937-957, <https://doi.org/10.5194/gmd-11-937-2018>,  
620 2018.

621 Campbell, C. A.: Soil organic carbon, nitrogen, and fertility, *Dev. Soil Sci.*, 8, 173-271,  
622 [https://doi.org/10.1016/S0166-2481\(08\)70020-5](https://doi.org/10.1016/S0166-2481(08)70020-5), 1978.

623 Castro, H. F., Classen, A. T., Austin, E. E., Norby, R. J., and Schadt, C. W.: Soil  
624 Microbial Community Responses to Multiple Experimental Climate Change  
625 Drivers, *Appl. Environ. Microbiol.*, 76(4), 999-1007,  
626 <https://doi.org/10.1128/AEM.02874-09>, 2010.

627 Chandel, A. K., Jiang, L. F., and Luo, L. Q.: Microbial Models for Simulating Soil  
628 Carbon Dynamics: A Review, *J GEOPHYS RES- BIOGEO.*, 128(8),  
629 <https://doi.org/10.1029/2023JG007436>, 2023.

630 Chen, J., Luo, YQ., van Groenigen, KJ., Hungate, BA., Cao, JJ., Zhou, XH., and  
631 Wang, RW.: A keystone microbial enzyme for nitrogen control of soil carbon  
632 storage, *Sci. Adv.*, 4(8), <https://doi.org/10.1126/sciadv.aag1689>, 2018.

633 Choat, B., Brodribb, T. J., Brodersen, C. R., Duursma, R. A., López, R., and Medlyn,  
634 B. E.: Triggers of tree mortality under drought, *NATURE.*, 558(7711), 531-539,  
635 <https://doi.org/10.1038/s41586-018-0240-x>, 2018.

636 Citerne, N., Wallace, H. M., Lewis, T., Reverchon, F., Omidvar, N., Hu, H. W., Shi, X.  
637 Z., Zhou, X. H., Zhou, G. Y., Farrar, M., Rashti, M. R., and Bai, S. H.: Effects of  
638 Biochar on Pulse C and N Cycling After a Short-term Drought: a Laboratory Study,  
639 *J. Soil Sci. Plant Nutr.*, 21(4), 2815-2825, [https://doi.org/10.1007/s42729-021-](https://doi.org/10.1007/s42729-021-00568-z)  
640 [00568-z](https://doi.org/10.1007/s42729-021-00568-z), 2021.

641 Cotrufo, M. F., and Lavalley, J. M.: Soil organic matter formation, persistence, and  
642 functioning: A synthesis of current understanding to inform its conservation and  
643 regeneration, *Adv. Agron.*, 172, 1-66,  
644 <https://doi.org/10.1016/bs.agron.2021.11.002>, 2022.

645 Cotrufo, M. F., Ranalli, M. G., Haddix, M. L., Six, J., and Lugato, E.: Soil carbon  
646 storage informed by particulate and mineral-associated organic matter, *Nat.*  
647 *Geosci.*, 12(12), 989-994, <https://doi.org/10.1038/s41561-019-0484-6>, 2019.

648 Cotrufo, M. F., Wallenstein, M. D., Boot, C. M., Deneff, K., and Paul, E.: The Microbial  
649 Efficiency-Matrix Stabilization (MEMS) framework integrates plant litter  
650 decomposition with soil organic matter stabilization: do labile plant inputs form  
651 stable soil organic matter? *Glob Chang Biol.*, 19(4), 988-95,  
652 <https://doi.org/10.1111/gcb.12113>, 2013.

653 de Vries, FT., Griffiths, RI., Bailey, M., Craig, H., Girlanda, M., Gweon, HS., Hallin,  
654 S., Kaisermann, A., Keith, AM., Kretschmar, M., Lemanceau, P., Lumini, E.,  
655 Mason, KE., Oliver, A., Ostle, N., Prosser, JI., Thion, C., Thomson, B., Bardgett,  
656 RD.: Soil bacterial networks are less stable under drought than fungal networks,  
657 *Nat. Commun.*, 9, <https://doi.org/10.1038/s41467-018-05516-7>, 2018.

658 Du, F. F., Zhang, Y. M., Zhou, L. Y., Dietrich, P., Zhou, G. Y., Wang, J., Zhang, Q. Z.,  
659 Wang, X. C., Du, Z. G., and Zhou, X. H.: Similar carbon accumulation rates with

660 distinct drivers in two temperate forest restoration approaches, *CATENA.*, 258,  
661 <https://doi.org/10.1016/j.catena.2025.109249>, 2025.

662 Du, Z. G., Nie, Y. Y., He, Y. H., Yu, G. R., Wang, H. M., and Zhou, X. H.:  
663 Complementarity of flux- and biometric-based data to constrain parameters in a  
664 terrestrial carbon model, *TELLUS B.*, 67,  
665 <https://doi.org/10.3402/tellusb.v67.24102>, 2015.

666 Du, Z. G., Zhou, X. H., Shao, J. J., Yu, G. R., Wang, H. M., Zhai, D. P., Xia, J. Y., and  
667 Luo, YQ.: Quantifying uncertainties from additional nitrogen data and processes  
668 in a terrestrial ecosystem model with Bayesian probabilistic inversion, *Adv. Model.*  
669 *Earth Syst.*, 9(1), 548-565, <https://doi.org/10.1002/2016MS000687>, 2017.

670 Eastman, B. A., Wieder, W. R., Hartman, M. D., Brzostek, E. R., Peterjohn, and W. T.  
671 Can models adequately reflect how long-term nitrogen enrichment alters the forest  
672 soil carbon cycle? *BIOGEOSCIENCES.*, 21(1), 201-221,  
673 <https://doi.org/10.5194/bg-21-201-2024>, 2024.

674 Evans, C. D., Monteith, D. T., and Cooper, D. M.: Long-term increases in surface water  
675 dissolved organic carbon: Observations, possible causes and environmental  
676 impacts, *Environ. Pollut.*, 137(1), 55-71,  
677 <https://doi.org/10.1016/j.envpol.2004.12.031>, 2005.

678 Ficken, C. D., and Warren, J. M.: The carbon economy of drought: comparing  
679 respiration responses of roots, mycorrhizal fungi, and free-living microbes to an  
680 extreme dry-rewet cycle, *PLANT SOIL.*, 435(1-2), 407-422,  
681 <https://doi.org/10.1007/s11104-018-03900-2>, 2019.

682 Feng, J., Yao, Y., He, Y., Wang, P., Hu, H., and Zhang, S.: Hydraulic strategies of  
683 *Cunninghamia lanceolata* under drought are shaped by native drought conditions,  
684 *For. Res.*, 5, e031, doi: <https://doi.org/10.48130/forres-0025-0031>. 2025.

685 Gao, Q., Hasselquist, N. J., Palmroth, S., Zheng, Z. M., and You, W. H.: Short-term  
686 response of soil respiration to nitrogen fertilization in a subtropical evergreen  
687 forest, *Soil Biol Biochem.*, 76, 297-300,  
688 <https://doi.org/10.1016/j.soilbio.2014.04.020>, 2014.

689 Guo, X. W., Rossel, R. A. V., Wang, G. C., Xiao, L. J., Wang, M. M., Zhang, S., and  
690 Luo, Z. K.: Particulate and mineral-associated organic carbon turnover revealed  
691 by modelling their long-term dynamics, *Soil Biol Biochem.*, 173,  
692 <https://doi.org/10.1016/j.soilbio.2022.108780>, 2022.

693 Han, Y. A., Deng, J. J., Zhou, W. M., Wang, Q. M., and Yu, D. P.: Seasonal Responses  
694 of Hydraulic Function and Carbon Dynamics in Spruce Seedlings to Continuous  
695 Drought, *Front. Plant Sci.*, 13, <https://doi.org/10.3389/fpls.2022.868108>, 2022.

696 Hansen, P. M., Even, R., King, A. E., Lavalley, J., Schipanski, M., and Cotrufo, M. F.:  
697 Distinct, direct and climate-mediated environmental controls on global particulate  
698 and mineral-associated organic carbon storage, *Glob Chang Biol.*, 30(1),  
699 <https://doi.org/10.1111/gcb.17080>, 2024.

700 Hao, X. C., and Singh, V. P.: Drought characterization from a multivariate perspective:  
701 A review, *J. Hydrol.*, 527, (668-678),  
702 <https://doi.org/10.1016/j.jhydrol.2015.05.031>, 2015.

703 Honeker, L. K., Pugliese, G., Ingrisch, J., Fudyma, J., Gil-Loaiza, J., Carpenter, E.,

704 Singer, E., Hildebrand, G., Shi, L. L., Hoyt, D. W., Chu, R. K., Toyoda, J.,  
705 Krechmer, J. E., Claflin, M. S., Ayala-Ortiz, C., Freire-Zapata, V., Pfannerstill, E.  
706 Y., Daber, L. E., Meeran, K., Dippold, M. A., Kreuzwieser, J., Williams, J., Ladd,  
707 S. N., Werner, C., Tfaily, M. M., and Meredith, L. K.: Drought re-routes soil  
708 microbial carbon metabolism towards emission of volatile metabolites in an  
709 artificial tropical rainforest, *Nat. Microbiol.*, 9(4), 1146-1147,  
710 <https://doi.org/10.1038/s41564-023-01507-7>, 2024.

711 Huang, Y., Guenet, B., Ciais, P., Janssens, I. A., Soong, J. L., Wang, Y. L., Goll, D.,  
712 Blagodatskaya, E., and Huang, Y. Y.: ORCHIMIC (v1.0), a microbe-mediated  
713 model for soil organic matter decomposition, *Geosci. Model Dev.*, 11(6), 2111-  
714 2138, <https://doi.org/10.5194/gmd-11-2111-2018>, 2018.

715 Hueso, S., García, C., and Hernández, T.: Severe drought conditions modify the  
716 microbial community structure, size and activity in amended and unamended soils,  
717 *Soil Biol Biochem.*, 50(167-173), <https://doi.org/10.1016/j.soilbio.2012.03.026>,  
718 2012.

719 IPCC, 2023: Climate Change 2023: Synthesis Report. Contribution of Working Groups  
720 I, II and III to the Sixth Assessment Report of the Intergovernmental Panel on  
721 Climate Change [Core Writing Team, H. Lee and J. Romero (eds.)]. IPCC, Geneva,  
722 Switzerland, pp. 35-115, doi: 10.59327/IPCC/AR6-9789291691647.

723 Jenny, H.: Factors of soil formation, McGraw-Hill, New York, 1941.

724 Jiang Z, Fu Y, Zhou L, He Y, Zhou G, Dietrich P, Long J, Wang X, Jia S, Ji Y, Jia Z,  
725 Song B, Liu R, Zhou X.: Plant growth strategy determines the magnitude and  
726 direction of drought-induced changes in root exudates in subtropical forests, *Glob  
727 Chang Biol.*, 29, 3476-3488, 2023.

728 Knorr, W., Prentice, I. C., House, J. I., and Holland, E. A.: Long-term sensitivity of soil  
729 carbon turnover to warming, *NATURE.*, 433(7023), 298-301,  
730 <https://doi.org/10.1038/nature03226>, 2005.

731 Krinner, G., Viovy, N., de Noblet-Ducoudré, N., Ogée, J., Polcher, J., Friedlingstein, P.,  
732 Ciais, P., Sitch, S., and Prentice, I. C.: A dynamic global vegetation model for  
733 studies of the coupled atmosphere-biosphere system -: art. no. GB1015, *Global  
734 Biogeochem. Cycles.*, 19(1), <https://doi.org/10.1029/2003GB002199>, 2005.

735 Lawrence, C. R., Neff, J. C., and Schimel, J. P.: Does adding microbial mechanisms of  
736 decomposition improve soil organic matter models? A comparison of four models  
737 using data from a pulsed rewetting experiment, *Soil Biol Biochem.*, 41(9), 1923-  
738 1934, <https://doi.org/10.1016/j.soilbio.2009.06.016>, 2009.

739 Lawrence, D. M., Fisher, R. A., Koven, C. D., Oleson, K. W., Swenson, S. C., Bonan,  
740 G., Collier, N., Ghimire, B., van Kampenhout, L., Kennedy, D., Kluzek, E.,  
741 Lawrence, P. J., Li, F., Li, H. Y., Lombardozzi, D., Riley, W. J., Sacks, W. J., Shi,  
742 M. J., Vertenstein, M., Wieder, W. R., Xu, C. G., Ali, A. A., Badger, A. M., Bisht,  
743 G., van den Broeke, M., Brunke, M. A., Burns, S. P., Buzan, J., Clark, M., Craig,  
744 A., Dahlin, K., Drewniak, B., Fisher, J. B., Flanner, M., Fox, A. M., Gentine, P.,  
745 Hoffman, F., Keppel-Aleks, G., Knox, R., Kumar, S., Lenaerts, J., Leung, L. R.,  
746 Lipscomb, W. H., Lu, Y. Q., Pandey, A., Pelletier, J. D., Perket, J., Randerson, J.

747 T., Ricciuto, D. M., Sanderson, B. M., Slater, A., Subin, Z. M., Tang, J. Y., Thomas,  
748 R. Q., Martin, M. V., and Zeng, X. B.: The Community Land Model Version 5:  
749 Description of New Features, Benchmarking, and Impact of Forcing Uncertainty.  
750 *J. Adv. Model. Earth Syst.*, 11(12), 4245-4287.  
751 <https://doi.org/10.1029/2018MS001583>, 2019.

752 Lee, J., and Rossel, R. V. A.: Soil carbon simulation confounded by different pool  
753 initialization, *Nutr. Cycling Agroecosyst.*, 116(2), 245-255,  
754 <https://doi.org/10.1007/s10705-019-10041-0>, 2020.

755 Liang, C., Kästner, M., and Joergensen, R. G.: 2020. Microbial necromass on the rise:  
756 The growing focus on its role in soil organic matter development. *Soil Biol*  
757 *Biochem.*, 150, <https://doi.org/10.1016/j.soilbio.2020.108000>, 2020.

758 Lugato, E., Lavalley, JM., Haddix, ML., Panagos, P., Cotrufo, MF.: 2022. Different  
759 climate sensitivity of particulate and mineral-associated soil organic matter. *Nat.*  
760 *Geosci.*, 15(6), 509-509, <https://doi.org/10.1038/s41561-022-00945-y>, 2022.

761 Luo, Z. K., Luo, Y. Q., Wang, G. C., Xia, J. Y., and Peng, C. H.: Warming-induced  
762 global soil carbon loss attenuated by downward carbon movement. *Glob Chang*  
763 *Biol.*, 26(12), 7242-7254, <https://doi.org/10.1111/gcb.15370>, 2020.

764 Martiny, J. B. H., Jones, S. E., Lennon, J. T., and Martiny, A. C.: Microbiomes in light  
765 of traits: A phylogenetic perspective, *SCIENCE.*, 350(6261),  
766 <https://doi.org/10.1126/science.aac9323>, 2015.

767 Meir, P., Metcalfe, D. B., Costa, A. C. L., and Fisher, R. A.: The fate of assimilated  
768 carbon during drought: impacts on respiration in Amazon rainforests, *PHILOS T*  
769 *R SOC B.*, 363(1498), 1849-1855, <https://doi.org/10.1098/rstb.2007.0021>, 2008.

770 Moorhead, D. L., Sinsabaugh, R. L.: A theoretical model of litter decay and microbial  
771 interaction, *Ecol. Monogr.*, 76(2), 151-174, [https://doi.org/10.1890/0012-9615\(2006\)076\[0151:ATMOLD\]2.0.CO;2](https://doi.org/10.1890/0012-9615(2006)076[0151:ATMOLD]2.0.CO;2), 2006.

773 Müller, L. M., and Bahn, M.: Drought legacies and ecosystem responses to subsequent  
774 drought, *Glob Chang Biol.*, 28(17), 5086-5103. <https://doi.org/10.1111/gcb.16270>,  
775 2022.

776 Paul, E. A., and Van Vee, J. A.: The use of tracers to determine the dynamic nature of  
777 organic matter, *Trans. Int. Congr. Soil Sci.*, 11(3), 61-102, 1978.

778 Pennisi, E.: Global drought experiment reveals the toll on plant growth, *Science.*,  
779 377(6609), 901-910, <https://doi.org/10.1126/science.ade5540>. Epub 2022 Aug 25,  
780 2022.

781 Preece, C., Verbruggen, E., Liu, L., Weedon, J. T., and Peñuelas, J.: Effects of past and  
782 current drought on the composition and diversity of soil microbial communities,  
783 *Soil Biol Biochem.*, 131(28-39), <https://doi.org/10.1016/j.soilbio.2018.12.022>,  
784 2019.

785 Quiroga, G., Castagneyrol, B., Abdala-Roberts, L., and Moreira, X.: A meta-analysis of  
786 the effects of climate change-related abiotic factors on aboveground and  
787 belowground plant-associated microbes, *OIKOS.*, 2024(7),  
788 <https://doi.org/10.1111/oik.10411>, 2024.

789 Reinelt, L., Whitaker, J., Kazakou, E., Bonnal, L., Bastianelli, D., Bullock, JM., Ostle,  
790 NJ.: Drought effects on root and shoot traits and their decomposability, *Funct.Ecol.*,

791 37(4), 1044-1054, <https://doi.org/10.1111/1365-2435.14261>, 2023.

792 Ricks, K. D., and Yannarell, A. C.: Soil moisture incidentally selects for microbes that  
793 facilitate locally adaptive plant response, *P ROY SOC B-BIOL SCI.*, 290(2001),  
794 <https://doi.org/10.1098/rspb.2023.0469>, 2023.

795 Rowland, L., Ramírez-Valiente, J. A., Hartley, I. P., and Mencuccini, M.: How woody  
796 plants adjust above- and below-ground traits in response to sustained drought,  
797 *New Phytol.*, 239(4), 1173-1189, <https://doi.org/10.1111/nph.19000>, 2023.

798 Saiya-Cork, K. R., Sinsabaugh, R. L., and Zak, D. R.: The effects of long term nitrogen  
799 deposition on extracellular enzyme activity in an *Acer Saccharum* forest soil, *Soil  
800 Biol Biochem.*, 34(9), 1309-1315, [https://doi.org/10.1016/S0038-0717\(02\)00074-](https://doi.org/10.1016/S0038-0717(02)00074-3)  
801 [3](https://doi.org/10.1016/S0038-0717(02)00074-3), 2002.

802 Sardans, J., and Peñuelas, J.: Soil Enzyme Activity in a Mediterranean Forest after Six  
803 Years of Drought, *Soil Sci. Soc. Am. J.*, 74(3), 838-851,  
804 <https://doi.org/10.2136/sssaj2009.0225>, 2010.

805 Schimel, J. P.: Life in Dry Soils: Effects of Drought on Soil Microbial Communities  
806 and Processes, *ANNU REV ECOL EVOL S.*, 49, 409-432,  
807 <https://doi.org/10.1146/annurev-ecolsys-110617-062614>, 2018.

808 Schwalm, C. R., Anderegg, W. R. L., Michalak, A. M., Fisher, J. B., Biondi, F., Koch,  
809 G., Litvak, M., Ogle, K., Shaw, J. D., Wolf, A., Huntzinger, D. N., Schaefer, K.,  
810 Cook, R., Wei, Y. X., Fang, Y. Y., Hayes, D., Huang, M. Y., Jain, A., and Tian, H.  
811 Q.: Global patterns of drought recovery, *NATURE.*, 548(7666), 202-205,  
812 <https://doi.org/10.1038/nature23021>, 2017.

813 Si, Q., Chen, K., Wei, B., Zhang, Y., Sun, X., and Liang, J.: Formation of particulate  
814 organic carbon from dissolved substrate input enhances soil carbon sequestration,  
815 *EGUsphere.*, <https://doi.org/10.5194/egusphere-2023-1483>, 2023.

816 Sokol, N. W., Sanderman, J., and Bradford, M. A.: Pathways of mineral-associated soil  
817 organic matter formation: Integrating the role of plant carbon source, chemistry,  
818 and point of entry, *Glob Chang Biol.*, 25(1), 12-24,  
819 <https://doi.org/10.1111/gcb.14482>, 2019.

820 Sowerby, A., Emmett, B. A., Williams, D., Beier, C., and Evans, C. D.: The response of  
821 dissolved organic carbon (DOC) and the ecosystem carbon balance to  
822 experimental drought in a temperate shrubland, *Eur. J. Soil Sci.*, 61(5), 697-709,  
823 <https://doi.org/10.1111/j.1365-2389.2010.01276.x>, 2010.

824 Stursová, M., Zifčáková, L., Leigh, M. B., Burgess, R., and Baldrian, P.: Cellulose  
825 utilization in forest litter and soil: identification of bacterial and fungal  
826 decomposers, *FEMS Microbiol. Ecol.*, 80(3), 735-746,  
827 <https://doi.org/10.1111/j.1574-6941.2012.01343.x>, 2012.

828 Su, X., Su, X. L., Yang, S. C., Zhou, G. Y., Ni, M. Y., Wang, C., Qin, H., Zhou, X. H.,  
829 and Deng, J.: Drought changed soil organic carbon composition and bacterial  
830 carbon metabolizing patterns in a subtropical evergreen forest, *Sci. Total Environ.*,  
831 736, <https://doi.org/10.1016/j.scitotenv.2020.139568>, 2020a.

832 Su, X. L., Su, X., Zhou, G. Y., Du, Z. G., Yang, S. C., Ni, M. Y., Qin, H., Huang, Z. Q.,  
833 Zhou, X. H., and Deng, J.: Drought accelerated recalcitrant carbon loss by

834 changing soil aggregation and microbial communities in a subtropical forest, *Soil*  
835 *Biol Biochem.*, 148, <https://doi.org/10.1016/j.soilbio.2020.107898>, 2020b.

836 Szejgis, J., Carrillo, Y., Jeffries, T. C., Dijkstra, F. A., Chieppa, J., Horn, S., Bristol, D.,  
837 Maisnam, P., Eldridge, D., and Nielsen, U. N.: Altered rainfall greatly affects  
838 enzyme activity but has limited effect on microbial biomass in Australian dryland  
839 soils, *Soil Biol Biochem.*, 189, <https://doi.org/10.1016/j.soilbio.2023.109277>,  
840 2024.

841 Tiwari, T., Sponseller, R., and Laudon, H.: The emerging role of drought as a regulator  
842 of dissolved organic carbon in boreal landscapes, *Nat. Commun.*, 13(1),  
843 <https://doi.org/10.1038/s41467-022-32839-3>, 2022.

844 Tao, F., Houlton, B. Z., Huang, Y. Y., Wang, Y. P., Manzoni, S., Ahrens, B., Mishra, U.,  
845 Jiang, L. F., Huang, X. M., and Luo, Y. Q.: Convergence in simulating global soil  
846 organic carbon by structurally different models after data assimilation, *Glob*  
847 *Chang Biol.*, 30(5), <https://doi.org/10.1111/gcb.17297>, 2024.

848 Ulrich, DEM., Clendinen, CS., Alongi, F., Mueller, RC., Chu, RK., Toyoda, J.,  
849 Gallegos-Graves, L., Goemann, HM., Peyton, B., Sevanto, S., Dunbar, J.: Root  
850 exudate composition reflects drought severity gradient in blue grama (*Bouteloua*  
851 *gracilis*), *Sci.Rep.*, 12(1), <https://doi.org/10.1038/s41598-022-16408-8>, 2022.

852 Villarino, S. H., Pinto, P., Jackson, R. B., and Piñeiro, G.: Plant rhizodeposition: A key  
853 factor for soil organic matter formation in stable fractions, *Sci Adv.*, 7(16),  
854 <https://doi.org/10.1126/sciadv.abd3176>, 2021.

855 Wan, F., Bian, C., Weng, E., Luo, Y., and Xia, J.: TECO-CNP Sv1.0: A coupled carbon-  
856 nitrogen-phosphorus model with data assimilation for subtropical forests,  
857 *EGUsphere.*, <https://doi.org/10.5194/egusphere-2025-1243>, 2025.

858 Wang, XY., Lu, DL., Schonbeck, L., Han, YN., Bai, SB., Yu, DP., Han, QM., and Wang,  
859 QW.: Contrasting effects of prolonged drought and nitrogen addition on growth  
860 and non-structural carbohydrate dynamics in coexisting *Pinus koraiensis* and  
861 *Fraxinus mandshurica* saplings, *For. Res.*, 5, e003, [https://doi.org/10.48130/forres-](https://doi.org/10.48130/forres-0025-0002)  
862 [0025-0002](https://doi.org/10.48130/forres-0025-0002), 2025.

863 Wang, X, Zhou, L, Fu, Y, Jiang, Z, Jia, S, Song, B, Liu, D, and Zhou, X.: Drought-  
864 induced changes in rare microbial community promoted contribution of microbial  
865 necromass C to SOC in a subtropical forest, *Soil Biol Biochem.*, 189,  
866 <https://doi.org/10.1016/j.soilbio.2023.109252>, 2024.

867 Williams, A., de Vries, FT.: Plant root exudation under drought: implications for  
868 ecosystem functioning, *New Phytol.*, 225(5), 1899-1905,  
869 <https://doi.org/10.1111/nph.16223>, 2020.

870 Willard, S. J., Liang, G. P., Adkins, S., Foley, K., Murray, J., and Waring, B.: Land use  
871 drives the distribution of free, physically protected, and chemically protected soil  
872 organic carbon storage at a global scale, *Glob Chang Biol.*, 30(9),  
873 <https://doi.org/10.1111/gcb.17507>, 2024.

874 Wu, H., Peng, C., Moore, T. R., Hua, D., Li, C., Zhu, Q., Peichl, M., Arain, MA., and  
875 Guo, Z.: Modeling dissolved organic carbon in temperate forest soils: TRIPLEX-  
876 DOC model development and validation. *Geosci. Model Dev.*, 7(3), 867-881,  
877 <https://doi.org/10.5194/gmd-7-867-2014>, 2014.

878 Wu, R. Q., Wang, Y. S., Huo, X. Y., Chen, W. J., and Wang, D. X.: Drought and  
879 vegetation restoration patterns shape soil enzyme activity and nutrient limitation  
880 dynamics in the loess plateau, *J. Environ. Manage.*, 374,  
881 <https://doi.org/10.1016/j.jenvman.2024.123846>, 2025.

882 Wu, J. F., Yao, H. X., Chen, X. H., and Chen, X. W.: Dynamics of dissolved organic  
883 carbon during drought and flood events: A phase-by-stages perspective, *Sci. Total*  
884 *Environ.*, 871, <https://doi.org/10.1016/j.scitotenv.2023.162158>, 2023.

885 Wu, XW., Luo, YQ., Weng, ES., White, L., Ma, Y., Zhou, XH.: Conditional inversion  
886 to estimate parameters from eddy-flux observations, *J. Plant Ecol.*, 2(2), 55-68,  
887 <https://doi.org/10.1093/jpe/rtp005>, 2009.

888 Xu, T., White, L., Hui, D. F., and Luo, Y. Q.: Probabilistic inversion of a terrestrial  
889 ecosystem model: Analysis of uncertainty in parameter estimation and model  
890 prediction, *Global Biogeochem. Cycles.*, 20(2),  
891 <https://doi.org/10.1029/2005GB002468>, 2006.

892 Yin, H., Zheng, H. W., Zhang, B., Tariq, A., Lv, G. H., Zeng, F. J., and Graciano, C.:  
893 Stoichiometry of C: N: P in the Roots of *Alhagi sparsifolia* Is More Sensitive to  
894 Soil Nutrients Than Aboveground Organs, *Frontiers in Plant Science*, 12,  
895 <https://doi.org/10.3389/fpls.2021.698961>. 2021.

896 Zhao, T. H., Yang, X., He, R., Shi, B. K., Gao, W. F., Ma, J. Y., and Sun, W.: Plant-soil  
897 microbe adaptive strategies reshape soil respiration components under multi-year  
898 precipitation frequency reduction and nitrogen addition in a semi-arid grassland,  
899 *Funct. Ecol.*, 39(9), 2370-2380, <https://doi.org/10.1111/1365-2435.70118>, 2025.

900 Zhou, G. Y., Zhou, X. H., Liu, R. Q., Du, Z. G., Zhou, L. Y., Li, S. S., Liu, H. Y., Shao,  
901 J. J., Wang, J. W., Nie, Y. Y., Gao, J., Wang, M. H., Zhang, M. Y., Wang, X. H.,  
902 and Bai, S. H.: Soil fungi and fine root biomass mediate drought-induced  
903 reductions in soil respiration, *Funct. Ecol.*, 34(12), 2634-2643,  
904 <https://doi.org/10.1111/1365-2435.13677>, 2020.

905 Zhou, X. Q., Chen, C. R., Wang, Y. F., Xu, Z. H., Duan, J. C., Hao, Y. B., and Smail,  
906 S.: Soil extractable carbon and nitrogen, microbial biomass and microbial  
907 metabolic activity in response to warming and increased precipitation in a semiarid  
908 Inner Mongolian grassland, *GEODERMA.*, 206, 24-31  
909 <https://doi.org/10.1016/j.geoderma.2013.04.020>, 2013.